Co-funded by the European Union

HyUSPRe

Hydrogen **U**nderground **S**torage in **P**orous **Re**servoirs

Experimental assessment on the potential for hydrogen sulphide generation from abiotic pyrite reduction during geological storage of hydrogen

Prepared by: Andrew Kilpatrick, University of Edinburgh
Aliakbar Hassanpouryouzband, University of Edinburgh
Katriona Edlmann, University of Edinburgh
Eric Craenmehr, TNO
Remco Groenenberg, TNO

Please cite this report as: Kilpatrick, A., Edlmann, K. & Groenenberg, R., 2023: Experimental assessment of the potential for hydrogen sulphide generation from abiotic pyrite reduction during geological storage of hydrogen, H2020 HyUSPRe project report. 43 pp.

This report represents HyUSPRe project deliverable number D2.2: Report on the assessment of the potential for contamination / H_2S souring of produced hydrogen over the lifetime of a storage site.

The HyUSPRe consortium

Funded by

Acknowledgement

This project has received funding from the Fuel Cells and Hydrogen 2 Joint Undertaking (now Clean Hydrogen Partnership) under grant agreement No 101006632. This Joint Undertaking receives support from the European Union's Horizon 2020 research and innovation programme, Hydrogen Europe and Hydrogen Europe Research.

Disclaimer

Executive summary

The hydrogen-driven reduction of pyrite to secondary pyrrhotite and subsequent generation of H_2S is a geochemical reaction of potential significance for underground storage of hydrogen in porous reservoirs. In such a storage scheme hydrogen may be injected into a reservoir containing pyrite within the primary mineralogy, where it can create, or enhance, reducing conditions under which this reaction may occur. The generation of H_2S would have implications for the quality of the gas-stream and might impact down-well and surface infrastructure materials and components, thus requiring cleaning of the gas-stream post- withdrawal to comply with quality standards for injection into the grid, and proper safety precautions to be in place.

A series of batch reaction experiments were carried out in order to characterise this reaction and the conditions under which it may occur. These experiments utilised varying methodologies (static vs. stirred batch experiments, gas and solid vs. liquid analysis), starting solids (pure pyrite systems, vs. pyrite with calcite buffer, vs. pyrite mixed with reservoir material), and were carried out across a range of pressure/temperature conditions (50–150°C and 30–200 bar pH_2).

The results give good evidence that the reduction of pyrite to pyrrhotite in H_2-rich environments can be extensive and rapid at temperatures over 120°C, with over 50% of the surface of the initial pyrite powder converted to pyrrhotite within a matter of days. The data gathered also show that H_2S was generated as a result of this reaction. Some evidence from the experiments also suggests that the reaction may be occurring at 80°C, albeit at a much-reduced rate.

The results from the experiments presented herein confirm that the reductive dissolution of pyrite could occur during storage of hydrogen in reservoirs. We recommend that the potential for this reaction to occur be taken in consideration during the selection and design of hydrogen stores, particularly in higher temperature (>80°C) reservoirs. We also recommend further experimental work to better characterise the reaction under conditions closer to those likely encountered in geological stores, along with modelling work to better understand the potential impacts at the field-scale. This work also highlights the need to better constrain the reaction at lower temperatures (60–100°C) which are more typical of sedimentary basin storage sites, but at which the reaction may proceed at rates difficult to observe on the timescales employed in this work.

About HyUSPRe

Hydrogen **U**nderground **S**torage in **P**orous **Re**servoirs

The HyUSPRe project researches the feasibility and potential of implementing large-scale underground geological storage for renewable hydrogen in Europe. This includes the identification of suitable porous reservoirs for hydrogen storage, and technical and economic assessments of the feasibility of implementing large-scale storage in these reservoirs to support the European energy transition to net zero emissions by 2050. The project will address specific technical issues and risks regarding storage in porous reservoirs and conduct an economic analysis to facilitate the decision-making process regarding the development of a portfolio of potential field pilots. A techno-economic assessment, accompanied by environmental, social, and regulatory perspectives on implementation will allow for the development of a roadmap for widespread hydrogen storage by 2050, indicating the role of large-scale hydrogen storage in achieving a zero-emissions energy system in the EU by 2050.

This project has two specific objectives. Objective 1 concerns the assessment of the technical feasibility, associated risks, and the potential of large-scale underground hydrogen storage in porous reservoirs for Europe. HyUSPRe will establish the important geochemical, microbiological, flow, and transport processes in porous reservoirs in the presence of hydrogen via a combination of laboratory-scale experiments and integrated modelling; and establish more accurate cost estimates to identify the potential business case for hydrogen storage in porous reservoirs. Suitable storage sites will be identified, and their hydrogen storage potential will be assessed. Objective 2 concerns the development of a roadmap for the deployment of geological hydrogen storage up to 2050. The proximity of storage sites to large renewable energy infrastructure and the amount of renewable energy that can be buffered versus time varying demands will be evaluated. This will form a basis for developing future scenario roadmaps and preparing for demonstrations.

Document information, revision history, approval status

Document information

Title:	Experimental assessment on the potential for hydrogen sulphide generation during geological storage of hydrogen.
Lead beneficiary:	UEDIN
Contributing beneficiaries:	TNO
Due date:	M27 [December 31st, 2023]
Dissemination level:	Public
Published where:	HyUSPRe website
Recommended citation:	Kilpatrick, A., Edlmann, K. & Groenenberg, R., 2023: Experimental assessment of the potential for hydrogen sulphide generation from abiotic pyrite reduction during geological storage of hydrogen, H2020 HyUSPRe project report. 43 pp.

Revision history

Version	Name	Delivery date	Summary of changes
V1	Kilpatrick, A.	19/09/2023	Outline draft
V2	Kilpatrick, A.	04/12/2023	Draft for final review
V3	Kilpatrick, A.	14/12/2023	Reviewer's comments added for team review
V4	Kilpatrick, A.	21/12/2023	Final version with reviewer comments addressed

Approval status

Role	Name	Delivery date
Deliverable responsible:	University of Edinburgh	
Task leader:	Andrew Kilpatrick	
WP leader:	Katriona Edlmann	2023.12.21
HyUSPRe lead scientist	Remco Groenenberg	2023.12.21
HyUSPRe consortium manager:	Holger Cremer	2023.12.21

Table of Content

1 Introduction

The transition to zero-carbon energy generation from renewable sources requires storing renewable energy intermittently in energy carrier molecules, such as hydrogen (H_2), to overcome imbalances between renewable energy supply and energy demand. Large-scale subsurface storage of H_2 in porous media, e.g. in globally abundant depleted gas fields and saline aquifers, is being considered as an alternative to expensive purpose-built storage containers aboveground.

While hydrogen gas generally has a lower reactivity than, for example, CO_2 it is certainly more reactive than natural gas. While a large body of experimental and modelling work has built up around investigating the geochemical impacts of geological storage of CO_2 over the last three decades (Bateman et al. 2011; Czernichowski-Lauriol et al. 2006), the lack of experimental data related to hydrogen storage means that key uncertainties remain around potential geochemical reactions in storage reservoirs. Generally, these relate to microbial reactions, but there are also several abiotic processes that remain of concern. One of these is the potential reduction of pyrite (FeS_2) to pyrrhotite (FeS) in the presence of hydrogen, a reaction that generates H_2S, a hazardous, toxic, and corrosive gas, and leads to loss of hydrogen. The uncertainties around the potential for this reaction to occur in storage reservoirs needs to be addressed as it may affect stored hydrogen quality and associated infrastructure.

The work presented herein aims to address some of these uncertainties via an experimental program exploring pyrite reactivity in hydrogen-rich systems, using a variety of approaches and across a range of conditions.

The following section provides some more background to the study along with identification of what previous work there has been in the area. Thereafter the methodology and results of the current study are presented and discussed, followed by a broader discussion of their implications in the context of hydrogen storage, learning outcomes, and possible further experimental work.

2 Background

During geological storage of hydrogen, a key consideration is the integrity and containment of the hydrogen stored. This consideration encompasses losses of hydrogen from the store due to physical processes (i.e., migration and leakage), but, vitally, must also include the chemical reactivity of the hydrogen itself which may generate toxic reaction products as well. Biogeochemical processes may induce loss of hydrogen and production of unwanted reaction products through:

- Biotic utilisation of hydrogen, via hydrogenotrophic methanogenesis, acetogenesis or sulphate reduction (Ahn et al. 2022);
- Dissolution of hydrogen into formation fluids and eventual migration away from the primary storage area;
- Abiotic reaction between stored hydrogen, formation brines, and reservoir minerals, leading to physiochemical changes to the reservoir, e.g., changes in porosity and permeability, and to the stored hydrogen itself, with generation of unwanted reaction products like H_2S.

Experience from storage of town gas (a mixture of hydrogen, carbon monoxide, carbon dioxide, methane, nitrogen and volatile hydrocarbons) in Ketzin (Germany) and Beynes (France) in the second half of the twentieth century (1950's to 1980's) provides context to the potential significance of geochemical interactions in underground hydrogen storage. In both cases, alterations to the composition of stored gas were observed. Bourgeois et al. (1979) suggest that the increased concentration of hydrogen sulfide observed at Beynes can be accounted for by the abiotic reduction of pyrite as opposed to the action of sulfate-reducing bacteria. Reitenbach et al. (2015) suggests that the hydrogen partial pressure (5–10 MPa), temperature (25°C), and alkalinity that characterize the Beynes storage site support this argument, although given the temperature at this site the available experimental evidence (e.g., Truche et al. (2010)) would not support this finding and it would seem more likely that biotic reactions have a stronger influence at these conditions. At Ketzin, gas losses in the order of 2×10^8 m^3 were observed between 1964 and 1985; the processes causing the gas loss and evolution of gas composition have not been identified but are not considered to be sufficiently explained by microbial degradation alone (Reitenbach et al., 2015). Recognizing though that CO, CO_2 and traces of sulfur present in town gases make them chemically more reactive than pure hydrogen, the experience with town gas storage cannot be directly applied to storage of pure hydrogen.

Despite increasing interest in geological storage of hydrogen in recent years and the fact that town gas was stored in porous reservoirs for many years, there is relatively little published experimental or field data on the geochemical aspects of hydrogen storage. One of the first studies on the geotechnical feasibility of subsurface hydrogen storage was conducted by Foh et al. (1979). The authors studied the chemical mono-mineral reactions between hydrogen and 15 minerals typical of subsurface reservoirs under conditions they considered representative of a subsurface reservoir (temperature of about 40 °C and pressure of ~14 Mpa). While generally concluding that underground storage of hydrogen could be conducted safely and economically, they did recognize that reactions between hydrogen and iron sulfide minerals like pyrite could lead to dissolution of the mineral, with loss of hydrogen and generation of H_2S as a consequence. Similarly, Carden and Paterson (1979) found no major physical or chemical problems associated with underground storage of hydrogen. They did, however, recognise the possibility of hydrogen reacting with sulphur in sulphur-bearing minerals, which, being exothermic, would result in severe overheating and release of poisonous H_2S. The absence of any observations regarding pyrite reduction and H_2S generation is likely related to the small change at the experimental conditions used in relation to the sensitivity of the analytical technique and suitability of the experimental set-up to avoid any H_2S loss.

Recently, Hassannayebi et al. (2019) undertook a multi-step geochemical modelling approach to study the hydrogen–brine–mineral interactions through equilibrium and kinetic batch simulations and concluded that because of the uncertainty due to a lack of reliable kinetic data, the risk of hydrogen loss and reduction in reservoir and caprock integrity associated with geochemical interactions with hydrogen cannot be ruled out.

One source of experimental data which does exist is from work done on geological storage of radioactive waste. In this setting hydrogen is generated through the corrosion of steel waste canisters and hence consideration of the long-term fate of hydrogen and its effects on the wider geochemistry of such systems is a key consideration in nuclear waste disposal. A key reaction identified for such systems is the reduction of primary pyrite to pyrrhotite in the presence of hydrogen, leading to loss of hydrogen through the generation of H_2S. As well as leading to loss of stored hydrogen, H_2S formation may lead to corrosion of storage infrastructure and changes to the geochemistry of the storage reservoir. The goal of this work, therefore, is to investigate, via experiments, the potential for pyrite reduction in the presence of hydrogen under conditions relevant to geological storage of hydrogen.

H_2S can be generated during reduction of pyrite to pyrrhotite as follows (see Equation 2.1):

$$FeS_2 + H_2 = FeS + H_2S \; (Eq.\ 2.1)$$

Truche et al. (2009) & Truche et al. (2010) undertook a series of experiments to study the kinetics of this reaction under hydrothermal conditions representative of nuclear waste repositories and found that when pyrite is exposed to hydrogen, it reduces to pyrrhotite, releasing sulphide anions into the solution that can bond with hydrogen to form H_2S. Their work consisted of batch reaction experiments performed under slightly alkaline conditions with pyrite, hydrogen, and calcite-buffered solutions. At hydrogen partial pressures, ranging from 3 to 30 bar (~0.3-3 MPa) and temperatures, ranging from 90 to 180°C, they observed a partial transformation of pyrite to pyrrhotite via a coupled dissolution-precipitation reaction. Truche et al. (2013) reported the reduction of pyrite and subsequent pyrrhotite precipitation at temperatures at 90°C and higher as the dominant hydrogen-induced geochemical disturbance in clay-rich rocks, and suggest that temperature is one of the main driving forces in hydrogen-induced pyrite reduction. They did not test at temperatures below 90°C and did not observe sulfide generation at pH below 5.

Pyrite is a common, though generally minor, mineral in sedimentary basins where anoxic conditions persist and hence is likely to occur in the primary assemblage of potential hydrogen storage sites. As previous work indicates that pyrite is one of the few minerals likely to exhibit significant reactivity with injected hydrogen, and since this reaction could lead to the generation of H_2S, it is vital that the potential for and rate of these reactions are understood. Truche et al. studied the reaction at temperatures higher than would be expected for all but the deepest hydrogen storage reservoirs, and (partial) pressures that are significantly lower than anticipated. This work aims to provide a complementary assessment to theirs for the potential for reduction of pyrite (and subsequent generation of H_2S) through a similar series of batch type experiments, but under generic hydrogen storage conditions (40–150°C and 30–200 bar pH_2, and pH 7-9).

3 Methodology & Results

Hereafter the results are presented of two sets of batch reaction experiments designed to investigate the potential for reduction of pyrite to pyrrhotite, and subsequent H_2S generation, during geological storage of H_2. The approaches taken in these two sets of experiments are different and were chosen to provide complimentary sets of results, as well as being partially dictated by the equipment and facilities available within the respective organisations.

Both sets of experiments used batch reaction vessels: the experiments carried out at TNO utilised relatively low volume reactors fitted with stirring apparatus, while those carried out at UEDIN utilized large volume vessels, capable of holding multiple experiments at once, but with no facility for mixing. These approaches are distinguished as “stirred” and “static”, respectively, in the more detailed methodologies presented in the following sections. The “stirred” approach is the one more commonly used in fluid-rock interaction experiments (like those of Truche et al., 2010, 2013) as it ensures the experimental system is well mixed and that all of the surface area of the rock/mineral sample is available to the fluid for interaction.

The large volume, static reactor approach has the advantage of allowing multiple experiments to be carried out in a single reactor under identical pressure and temperature conditions. There is however a risk, that, without mixing, reactions (dissolution of hydrogen into the liquid, dissolution of the pyrite surface, for example) become diffusion-limited and that the whole surface of the solid sample is not available to the fluid for reaction. In addition, the gas phase for these experiments is not isolated per single experiment and interaction could take place. This static approach, therefore, is not suitable for deducing reaction rates, but may be successful in capturing the general magnitude and direction of reactions for a large number of experimental systems, while the stirred approach allows for more detailed investigation into the nature of reactions and their rates.

The experimental approaches also differed in the analysis of system components following reaction. The focus in the stirred experiments was on detailed analysis of the solids following reaction in order to identify changes in the solid itself (i.e., dissolution of pyrite, formation of pyrrhotite) via SEM and XRD, together with some analysis of the gas headspace within the experiments in order to monitor for formation of H_2S.

For the static experiments, meanwhile, the focus was on changes in fluid chemistry, with fluid samples collected at the end of runs and analysed for a broad suite of elemental concentrations via ICP-OES. The analytical approaches largely compliment the style of experiments: the SEM and XRD work on solids from the stirred experiments allowed detailed identification and quantification of mineral changes, though the analysis is time consuming, while ICP-OES analysis allowed relatively rapid identification of broad changes in fluid chemistry in the static experiments.

3.1 Stirred batch experiments (TNO)

3.1.1 Materials and Methods

Pyrite powder is supplied by Q-mineral (purity 98.0 % pyrite, 1,2 % pyrrhotite, 0,8 % other; sieved to particles size ≤ 40 microns). The other chemicals are supplied by Merck, hydrochloric acid (HCl 37 %), sodium chloride (NaCl, >99.0 %) and calcite ($NaHCO_3$/Na_2CO_3). The gasses; nitrogen (N_2 6.0 = 99.9999% purity), hydrogen (H_2 5.0 = 99,999% purity) and hydrogen sulphide (H_2S) 200 ppm in N_2, are supplied by Air Products. Deionized water is produced by

an integral water purification system at the High Tech Campus where the Material Solutions lab of TNO is located and used from the tap as such.

Experiments were carried out in stirred 185 ml stainless steel autoclave reactors (Premex SS) with Dursan coating or with a custom-made Teflon liner inside. Fitted heaters (Premex) around the autoclave come with a thermocouple to ensure accurate heating. The reactors are designed for high temperature and high pressure with a maximum T, P of resp. 150 °C and 350 bar and are manufactured from austenitic industrial stainless-steel grade X5NiCrTi26-15, also known as 1.4980/660/A286/UNS S66286, which is a special grade for heat resistant steel with high strength and high oxidation resistance. The reactor cover is made from the same stainless steel featured with a gas in- and outlet, safety valve and pressure gauge. A compressor designed for explosive gasses (Booster DLE 30 1-2 by Maximator) is used to generate the high-pressure values of hydrogen. Reacted samples are analysed by gas-chromatography coupled with mass spectrometry (GC-MS, Interscience), X-ray diffraction spectroscopy (XRD, Panalytical) with Rietveld refinement, and Scanning Electron Microscopy (SEM, FEI Quanta600) equipped with Energy Dispersive Spectroscopy (EDX, Ametek EDAX). The sample is centrifuged with a Multifuge 3L-R from Heraeus. Pyrite is milled by a milling apparatus (Dispermat SL C-5 by VMA Getzmann) and analysed by a particle size analyser (Mastersizer 3000 by Malvern Panalytical).

3.1.2 Experimental Design and Strategy

The reaction of hydrogen-induced abiotic pyrite reduction ($FeS_2 + H_2$ -> $FeS + H_2S$) is studied under environmental conditions representative for geological porous reservoirs in Europe (T-range 40-150 °C, P-range 30-200 bar). In a typical experiment (see Figure 1), pyrite powder is continuously stirred in brine by a coated magnetic stir bar inside an autoclave reactor. The headspace inside the reactor above the brine is filled with pure hydrogen gas at the required pressure, and the autoclave itself is continuously heated to maintain the required temperature. The pyrite powder, being continuously submerged in the brine, is exposed to (and reacts with) the hydrogen that is dissolved in the brine. After exposure for the duration of the experiment, the amount of pyrite converted to pyrrhotite is measured in three ways: 1) by measuring the gas head space with GC-MS to detect the presence of H_2S, a key reaction product; 2) by measuring the reacted powder with XRD and applying Rietveld refinement to quantify the ratio pyrite-to-pyrrhotite of the powder; and 3) by analysing the composition of the powder after reaction with SEM-EDX. In a first series of experiments, the aim was to test the set-up, and to explore at which P, T conditions the reaction actually occurs by analysing qualitatively the gas head space in the autoclave reactor as well as the reacted powder, resp. with GC-MS and XRD (without Rietveld refinement). Based on the findings from the first series, a second series of experiments was executed with different durations during which temperature, pressure and grain size were systematically varied to quantify reaction rates and their dependence on T, P, and grain size (proxy for surface area). After these experiments, the solid residue was quantitatively analysed by XRD with Rietveld refinement and SEM equipped with an EDX to obtain the composition of the residue (ratio pyrite vs. non-pyrite) and detect any morphological changes to the particles that would be evidence for the reaction to have occurred.

Series 1: Exploratory experiments to test pyrite reactivity at lower and upper conditions

In the first series of experiments, 200 mg pyrite particles (size up to 40 micron) were added to 38 ml brine (8 % NaCl) solution mixed with a pH buffer of pH 9 ($NaHCO_3/Na_2CO_3$) in a Teflon liner under nitrogen conditions. Prior to the addition of pyrite particles, the brine was bubbled with N_2 for 30 minutes to minimize the oxygen level. A magnetic stirrer was added into the Teflon liner and placed inside an autoclave reactor (Premex SS, Figure 2). The Teflon liner was closed with a lid equipped with an opening for gas sampling. To prevent ingress of free oxygen the sample preparations are done in a disposable glovebox under nitrogen.

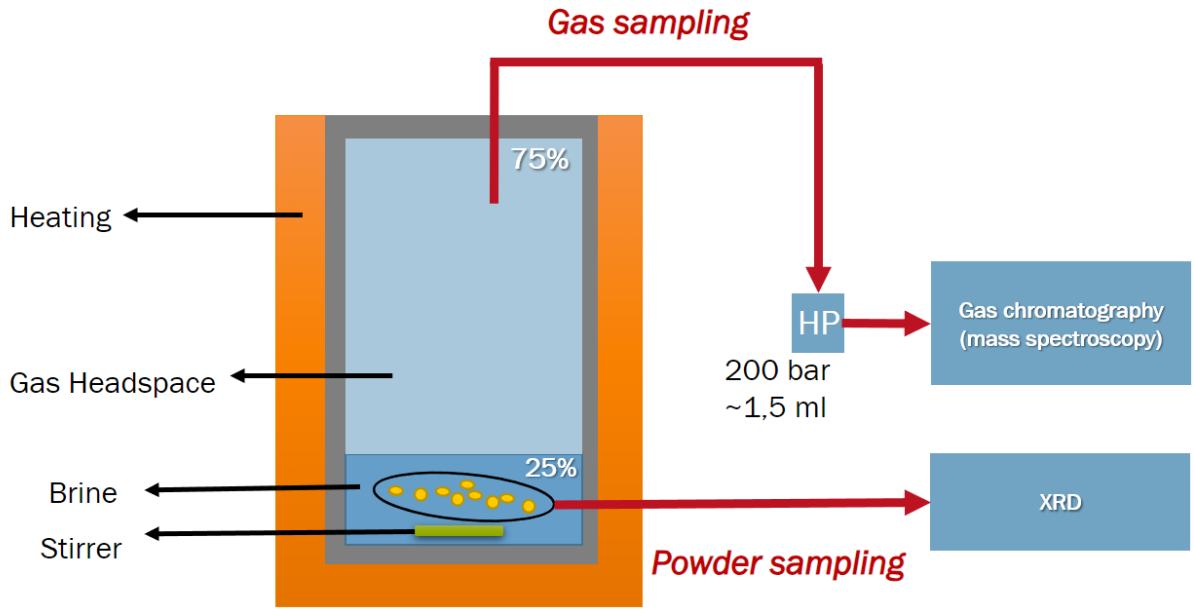

Figure 1. Simplified schematic representation of the experimental set-up of the reactor and analyses.

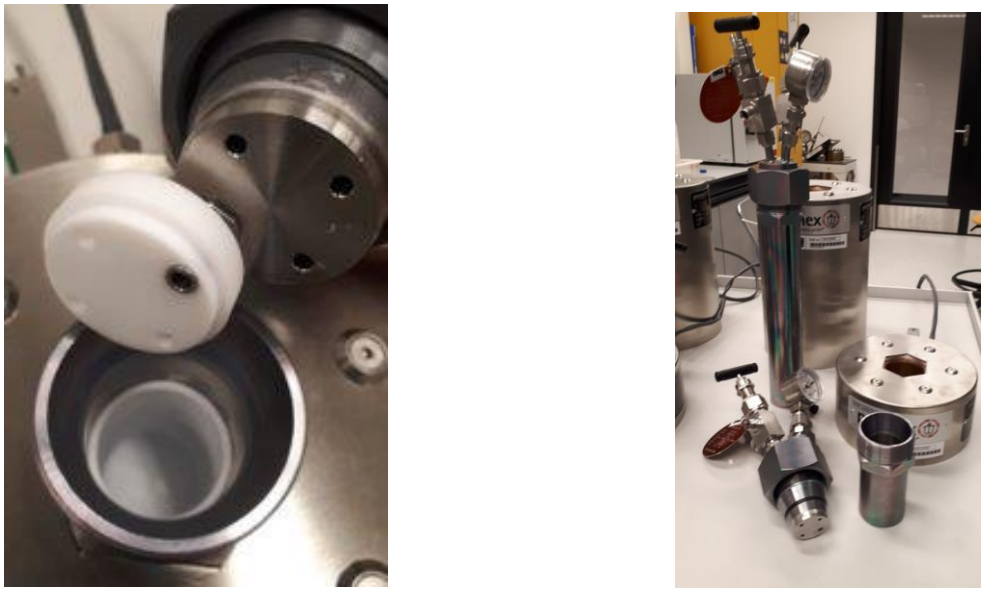

Figure 2. Premex SS reactors (of two different sizes) equipped with pressure/sample inlet/outlet, safety valve and pressure gauge. On the left with Teflon liner and on the right coated with Dursan coating.

Prior to H_2 injection, the reactor was pressurized 5 times to 15 bar N_2 to make sure no oxygen was present inside the reactor. Following this, hydrogen was introduced to the reactor and pressurized using the Maximator, the heater was turned on to reach the desired temperature, and the brine with pyrite powder was stirred at 150 rpm. After the designated reaction time (1 week) during which T and P were held at desired values, gas and powder samples were qualitatively analysed. After switching off the heating and the reactor had cooled down to room temperature gas samples were collected for GC-MS analysis by coupling an expansion tube to the reactor. Nitrogen was flushed through the expansion tube before and while coupling with the reactor, and the tube was made vacuum thereafter. By opening the valve between reactor and expansion tube the gas (mixture of H_2 and H_2S) flowed from the headspace inside the reactor into the expansion tube under high pressure. After gas sampling from the reactor, the

expansion tube was decoupled from the reactor and coupled to the GC-MS whereby the injection of the high-pressure gas mixture into the GC-MS was controlled by a mass flow controller (see Figure 1). To sample the reacted powder the reactor was slowly depressurised and opened under nitrogen whereafter the reacted powder sample (pyrite and solid reaction products) was separated from the brine by centrifugation, washed with deionized water, dried under a N_2 flow, and examined via XRD. All the steps were performed under a strict nitrogen atmosphere. It is worthwhile to mention that the pyrite particles were washed with 1 M HCl, followed by washing with deionized water five times, and dried overnight in a vacuum at 40 ^{0}C before the reaction. All the experiments were followed by a control experiment using N_2 instead of H_2.

Series 2: Systematic tests to quantify reaction rates and dependence on T, P and grain size

A second series of experiments was executed for quantitative analyses on the reacted powder after 1, 3 and 7 days, at pressures of 30 and 200 bar, temperatures of 40, 80, 120 and 150 °C, a pH of 9,0 (buffered), and particle sizes of 40 and 5 micron. The pyrite particle size was reduced using a top-down approach. Pyrite particles of size up to 40 microns were dispersed into a solution of (10 wt %) of NH_4OH and ground for 1.5 hours at 5000 rpm with 50 % power using 1 micron slit and 0.4 – 0.6 mm beads with a dispermat SL C-5 by VMA Getzmann. The particles size was analysed by a Mastersizer 3000 by Malvern Panalytical, the result of which indicated that the size of the 40 micron pyrite particles was successfully reduced to less than 5 micron.

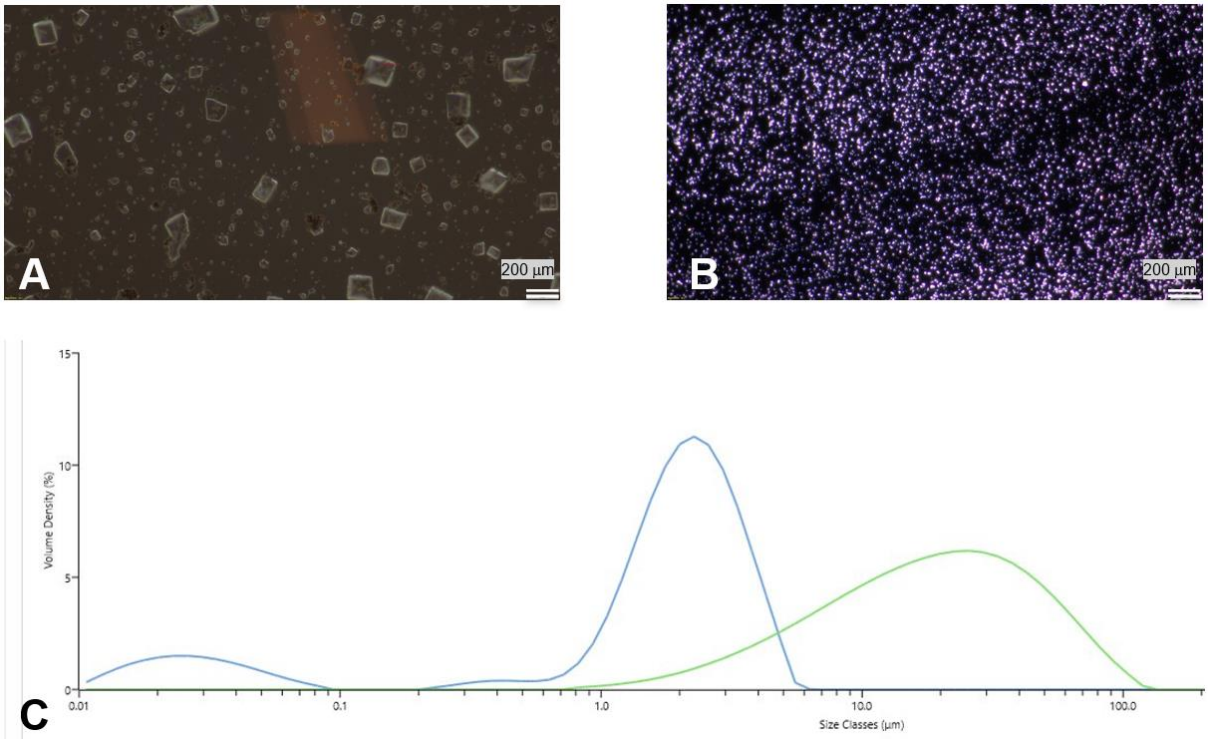

Figure 3. Shows the POM images of pyrite particles before (A) and after (B) milling process and the particle size plot of the Mastersizer (C).

Prior to the second series, the reactors were coated with an H_2S- and alkaline-resistant Dursan coating, thus avoiding the need for the Teflon liner. The Teflon liner was stained with reddish mineral compounds and was demonstrated to absorb significant amounts of H_2S, thus distorting the mass balance. In these experiments, 0.5 g of pyrite (Q-mineral, purity 98.0 %, up

to 40 micron) particles were added to 50 ml brine (8 % NaCl, pH 9,0 buffered) for each experiment. The analyses were done post-mortem on the dried powders with XRD followed by Rietveld refinement. For all other aspects the procedure of the first, qualitative, series was followed. Furthermore, the powder samples have been analysed by Scanning Electron Microscopy (SEM) equipped with Energy Dispersive Spectroscopy (EDX) to obtain the composition of the reacted powder (ratio pyrite vs. non-pyrite) and detect any morphological changes to the particles that would be evidence for the reaction to have occurred.

3.1.3 Measurements and Analysis

X-ray diffraction (XRD) analysis

Autoclave reactors were opened under nitrogen after cooling down to room temperature and pressure release. The sample was taken out and centrifuged with the Multifuge 3L-R at 4800 rpm for 5 minutes to collect the solid residue. The solid residue was dried under nitrogen and placed on the special powder sample holder whereafter it was measured with XRD followed by Rietveld refinement. Rietveld refinement is a technique used to characterise crystalline materials. It uses a least squares approach to refine a theoretical line profile until it matches the measured profile. To determine the peak intensity you have to take into account that the intensity depends on the structure factor, and can be calculated from the structural model for individual peaks. Therefore it can only be applied when specific atomic coordination in the unit cell and geometrical parameters are known and when a reasonable model exists for the structure. These parameters are in the library of the software wherewith the ratio of the different compounds can be calculated.

GC-MS sampling

Gas samples were collected at the end of the experiment using a sample tube connected to the reactor. The sample tube was flushed with N_2 and a vacuum introduced before it was filled with the high pressure reacted gas, from which a sample was then injected into the GC-MS. Before injection of the sample, the GC was flushed with N_2. Subsequently, the inlet valve of the GC was switched from N_2 to the sample tube. The pressure was controlled by the regulator to 1.25 bar and flushed for 30 seconds. Once the pressure dropped below 1.1 bar the injection into the GC was started. Inside the GC, all gasses were separated and only at the retention time of H_2S the valve to the MS was opened followed by gas flowing to the MS detector for analyses.

Scanning Electron Microscopy (SEM)

The reacted and dried powder samples were prepared on a sample holder to be transferred into the SEM. Typically, for each sample some representative spots are located. After making the SEM pictures the same spots are also measured with EDX. The EDX feature is especially appropriate for elemental analyses to detect the type of atoms in the sample. Once the molar ratio of iron (Fe) and sulphur (S) has been analysed it can be determined if pyrite (Fe_1S_2) has been reduced to pyrrhotite (Fe_1S_1)

Specific surface area by BET analyses

Nitrogen gas adsorption analyses by the Brunauer–Emmett–Teller (BET) method is the standard method to measure the specific surface area of solid materials. The BET or Langmuir surface area of a material is determined from the measurement of the physical adsorption of N_2-gas at different partial pressures (ISO 9277) by a Quantachrome Autosorb apparatus with Multiple point BET method. Sample preparation is executed by outgassing the powder for 2h at 200°C under high vacuum.

3.1.4 Stirred Batch Experiment Results

Series 1: Exploratory experiments to test pyrite reactivity at lower and upper extreme conditions

In the first series of experiments (see Table 1) 10 experiments were executed with pyrite exposed to high pressure: five with high H_2 pressure and five control experiments with high N_2 pressure. The series consists of buffered and non-buffered experiments, experiments at 80 and 150°C and experiments at 50 and 200 bar hydrogen. For all experiments at 150°C a pyrite conversion has been detected while the N_2 control experiments and the experiment at 80°C show no (detectable) conversion.

Table 1. Summary of results of pyrite reduction experiments in the first series after one week of exposure to hydrogen.

#	Particle size (μm)	pH	H2 pressure (bar)	Temperature (°C)	Result GC-MS	Result XRD
A	<40	9, buffered	50	150	H_2S	Pyrrhotite
B	<40	9, buffered	200	150	H_2S	Pyrrhotite
C	<40	7, no buffer	200	150	H_2S	Pyrrhotite
D	<40	7, no buffer	200	80	n.a.	No pyrrhotite
E	<5	9, buffered	200	150	H_2S	Pyrrhotite

GC-MS

A typical chromatogram of H_2S is shown in Figure 4 (left graph). The reddish-coloured peak indicates H_2S presence and the second (non-coloured) peak in the graph could be SH^- or a (carrier) gas (N_2/O_2). The GC cannot baseline separate H_2S from this second gas. The MS diagram (Figure 4, right graph) confirms that the highlighted peak is H_2S, as the typical molar mass distribution of H_2S is measured.

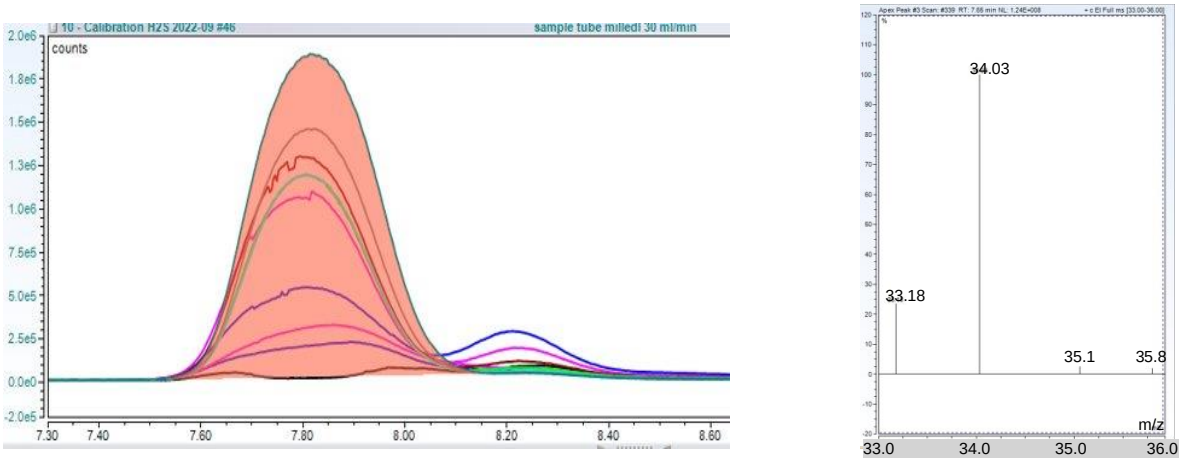

Figure 4. Illustrative GC-MS measurement that signals H_2S presence. On the left the highlighted peak represents the amount of counts for H_2S and on the right the MS diagram with the typical molar mass distribution of H_2S.

XRD

The outcome of the XRD measurements show complementary results. Several clear peaks of the different pyrrhotite phases show up in all experiments, except for the experiment at 80 °C (and the reference experiments with N_2) where no pyrrhotite is detected. The pyrite and pyrrhotite peaks at 2 theta angle (°) do not overlap and are therefore easy to recognize, as visualized in Figure 5.

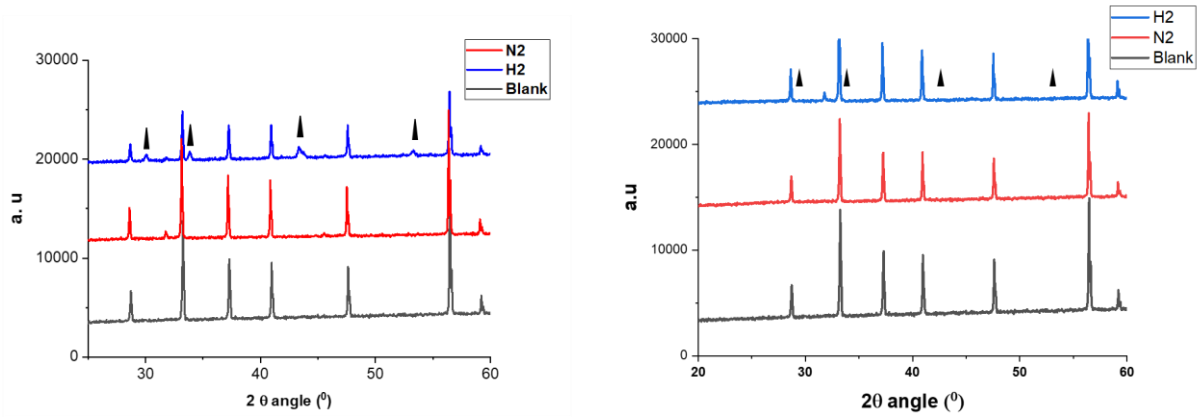

Figure 5. XRD results of two experiments, one showing evidence of conversion to pyrrhotite (left, #B in Table 1), and one showing no evidence of conversion (right, #D in table 1). Each XRD graph shows the result of XRD analyses of pyrite powder from 3 experiments: 1) unreacted virgin pyrite, black line; 2) pyrite exposed to nitrogen, red line; 3) pyrite exposed to hydrogen, blue line. The black triangles denote diffraction angles that ae are typical of pyrrhotite. In experiment #B (left), peaks in the blue line can be observed at the locations of the black triangles, while in experiment #D (right), no peaks are present in the blue line at these locations.

Series 2: Systematic tests to quantify reaction rates and dependence on T, P and grain size

In the second series of experiments (Table 2), pyrite exposure to hydrogen was tested systematically at a range of temperatures (40, 80, 120 and 150 °C) and pressures (30 and 200 bar). The pH of the brine (8% NaCl salinity) in all experiments was kept at pH~9 with a buffer, and all experiments were conducted with durations of 1, 3 and 7 days. Most experiments were conducted at 200 bar pressure, except for one experiment, which was conducted at 30 bar (and 120 °C). Likewise, in all experiments, <40 micron pyrite particles were used, except for one experiment, in which <5 micron pyrite particles were used (at 200 bar, 120 °C). A control experiment with N_2 was conducted at max. T (150 °C) and P (200 bar), the most favourable conditions for the reaction to occur. The whole series was quantitatively analysed by XRD with Rietveld refinement and by SEM equipped with EDX to obtain the composition of the reacted powder (ratio pyrite vs. non-pyrite) and detect any morphological changes to the particles that would be evidence for the reaction to have occurred.

Table 2. Conditions of the second series of experiments for quantitative analyses (in buffered brine with pH~9).

#	size	H_2 P (bar)	T (°C)	Exposure time (days)	Comments
9	<40	200	150	1, 3, 7	High T, test maximum conversion
9b	<40	200, N_2	150	1, 3, 7	N_2, control experiment
1a	<40	200	120	1, 3, 7	Reference P, T
4	<40	200	80	1, 3, 7	Medium T
2	<40	200	40	1, 3, 7	Minimum T
3	<40	30	120	1, 3, 7	Minimum P
5	<5	200	120	1, 3, 7	Higher surface area

SEM

While the unreacted virgin powder has a cubical crystal structure (Type I) with flat surfaces, the reacted powder has these flat surfaces with on top, newly grown, small irregular shaped crystals (Type II), see Figure 6, 7 and 8. It is clearly visible that the surfaces have been roughened by growth of crystals of Type II on the surfaces of crystals Type I. Similar observations were made by Truche et al. (2010). For representative spots the molar ratio of

iron (Fe) and sulphur (S) was analysed by EDX, which resulted in an average molar ratio of $Fe_1S_{1,14}$ ($Fe_{0,88}S_1$), while the starting value of the (unexposed) pyrite was $Fe_1S_{2,19}$ This indicates that a significant amount of pyrite (Fe_1S_2) has been reduced to pyrrhotite ($Fe_{(1-x)}S$, with x ranging 0-0.125) and/or troilite ($Fe_{(1-x)}S$, with x ranging 0-0.2; Iron-rich end-member of the pyrrhotite group), which is confirmed by the results of the XRD analyses (see further down).

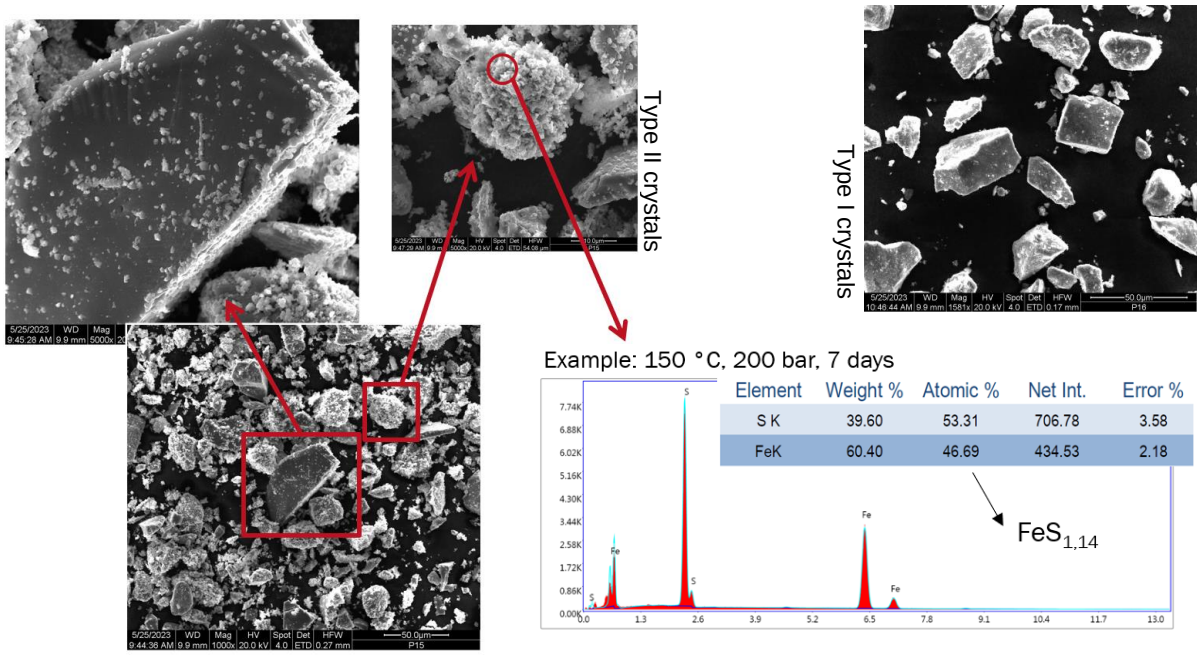

Figure 5. SEM pictures of reacted pyrite powder (left) and the results of the elemental analyses of typical spots by EDX (right). In the top right a picture of unreacted powder is shown.

Similar SEM and EDX analyses were done on pyrite powder particles after 7 days of hydrogen exposure for three experiments: 1) 80 °C, 200 bar; 2) 120 °C, 30 bar; and 3) 150 °C, 200 bar. For the third experiment, SEM and EDX analyses were also done for 1 and 3 days exposure time. Furthermore, SEM and EDX analyses were done for the control experiment under nitrogen at 150 °C, 200 bar after 7 days exposure time. EDX analyses were done on the new crystals grown (Type II), and on the flat cubical crystal surfaces (Type I). The results of the SEM and EDX analyses are shown in Table 3. Clearly, the new crystals (Type II) consist of a higher content of pyrrhotite than the flat surfaces (Type I). However, the flat surfaces on the cubical pyrite crystals (Type I) also show some reduction into pyrrhotite, other than in the control experiment and the experiment at 80 °C.

Table 3. Results of EDX analyses on SEM pictures for second series of experiments.

Temperature	**Pressure**	**Exposure**	**Ratio x of FeS_x**		**Pyrrhotite**	
(°C)	**(bar)**	**time (days)**	**of new crystals**	**of flat surface**	**new crystals (Type II)**	**flat surface (Type I)**
80	200	7	2,29	2,30	no	no
120	30	7	1,40	1,98	yes	a bit
150	200	1	1,55	2,16	yes	no
150	200	3	1,43	2,17	yes	no
150	200	7	1,14	1,76	yes	yes
150	200, N_2	7	n.a.	2,33	n.a.	no

Figure 7 shows some representative SEM pictures for conditions at which no pyrrhotite was formed/observed. Smooth flat crystal surfaces (Type I) can be seen and EDX has detected that the iron (Fe) sulphur (S) ratio is similar to the virgin powder.

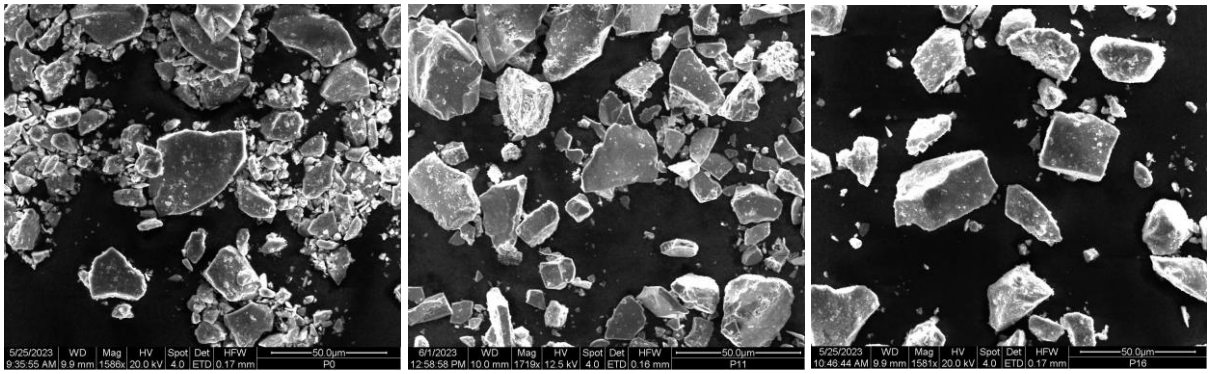

Figure 6. Unreacted pyrite crystals, Type I. From left to right: virgin powder, 80 °C experiment, control experiment with N_2. EDX shows that the white spots on flat surfaces are small pyrite particles, no pyrrhotite.

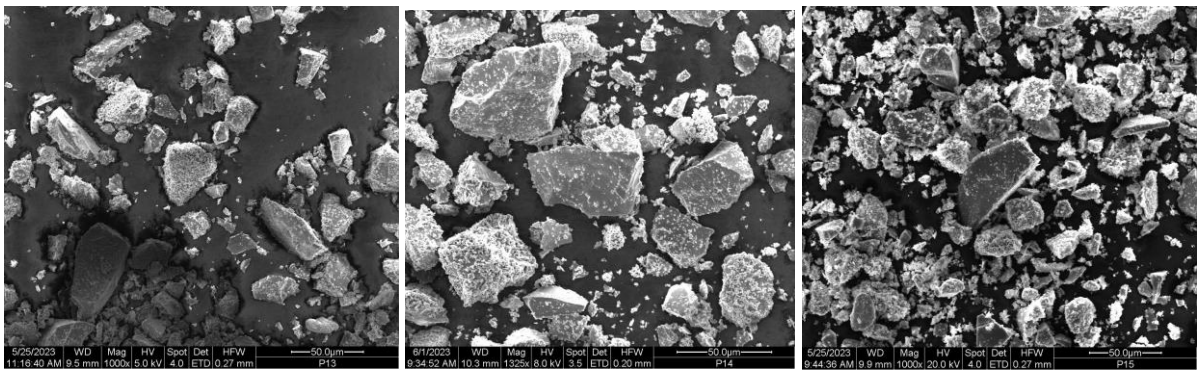

Figure 7. Reacted pyrite powder after exposure at 150 °C, 200 bar. From left to right: exposure after 1, 3 and 7 days. On flat crystal surfaces (Type I) white crystals (Type II) arise which are pyrrhotite. EDX shows that flat surfaces of Type I crystals are also partially reduced to pyrrhotite.

For comparison, Figure 8 shows reacted powder for conditions where pyrrhotite is formed. Many small crystal structures (Type II) cover the surface of the original clean areas of the pyrite crystals. The initially clean areas also show evidence of some reduction into pyrrhotite.

XRD

Rietveld refinement analyses were performed on the raw XRD data to determine the proportions of the various components in the reacted powder after exposure. Typically, graphs from the library of possibly present Fe-compounds in the sample, in this case pyrite, pyrrhotite, troilite, magnetite, and iron, were matched with the XRD graphs of the samples, giving an accurate composition of the ratio of the different components in the sample. The results of the XRD Rietveld analyses are shown in Figure 9 (bar chart) and Figure 10 (line graph), with the remark that residues of an unrecognized chemical bond that repeatedly appeared in the XRD graphs in extremely low quantities have been omitted.

A significant effect of temperature is observed. As temperature increases, the amount of pyrite in the reacted powder decreases, while the amounts of pyrrhotite and troilite increase. At 120 and 150 °C, the amounts of pyrrhotite and troilite are substantial, indicating that resp. ~13% and ~52% of pyrite has converted in 7 days. At 80°C though, amounts are comparable to those in the unreacted virgin (natural) pyrite powder obtained from the supplier (Q-mineral), i.e., ~ 2% for pyrrhotite and troilite together, hence a conclusion on whether the reaction occurred cannot

be firmly drawn, but if it did, it happened at a (much) slower rate. At 40 °C, amounts of pyrrhotite and troilite measured are well below the accuracy of the measurement method, and also lower than in the virgin unreacted powder. A possible hypothesis for this could be that the pyrrhotite and troilite that were present originally, changed from crystalline to amorphous phases which cannot be analysed by XRD. Another explanation could be that part of the pyrrhotite dissolved and was therefore not present in the reacted powder. Although this type of oxidative dissolution of pyrrhotite is only known to happen under acidic conditions or in the presence of oxygen (Belzile et al. 2004), and hence would not be expected in our experiments that are conducted under alkaline and anoxic conditions, it must also be noted that the mechanisms of oxidation of minerals like pyrite and pyrrhotite at a molecular level are complex and not fully understood. From microbial experiments it is known that bubbling of the brine with O_2 does not remove all oxygen, so this oxygen could have reacted with pyrrhotite. However, it is not clear why this did not occur in the N_2 experiments.

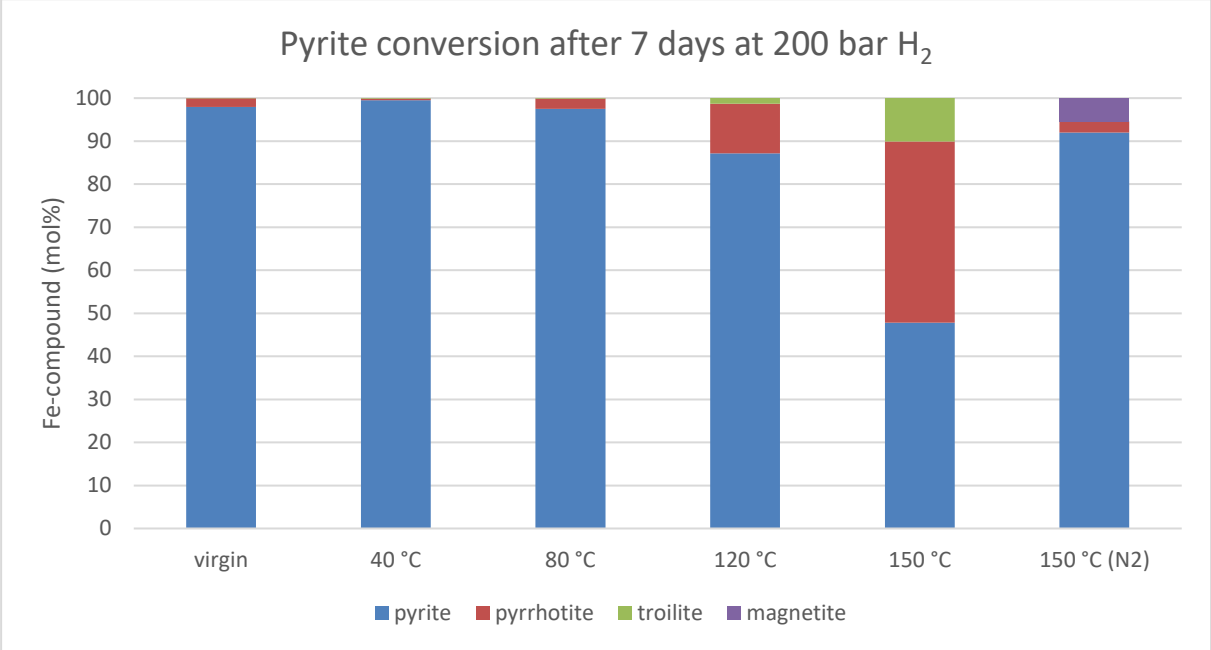

Figure 8. XRD Rietveld results after hydrogen exposure to pyrite at 200 bar.

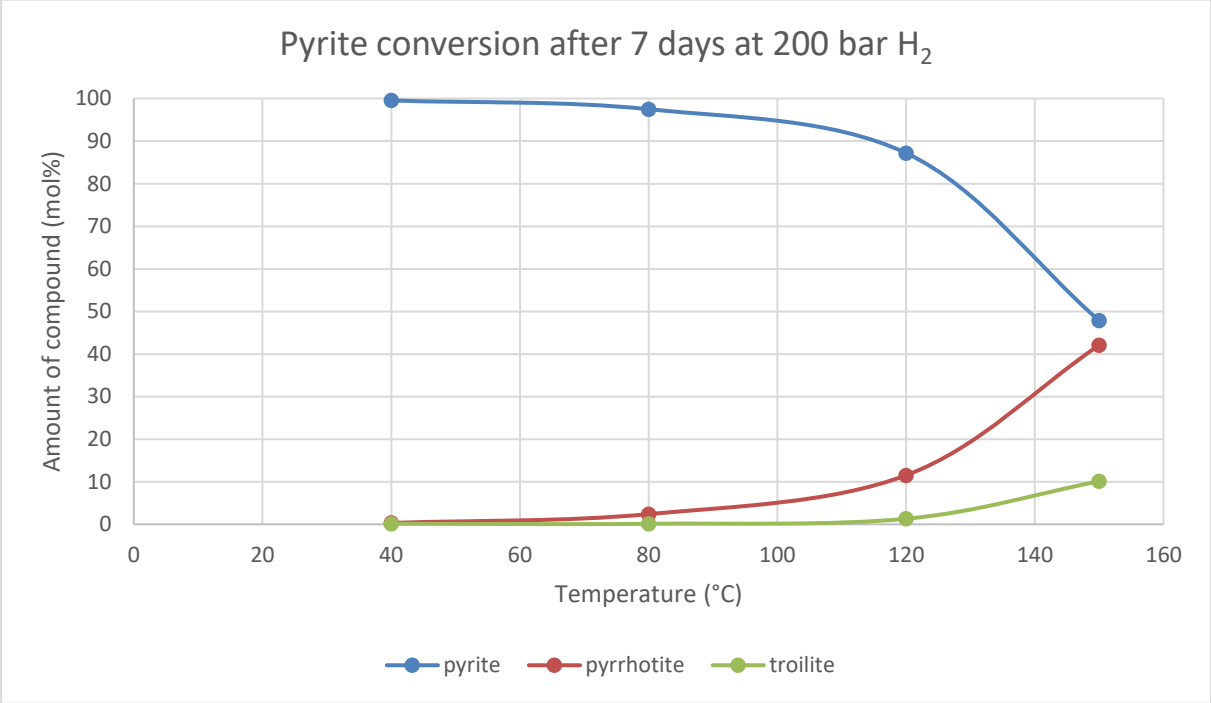

Figure 9. Composition in mol% is plotted against temperature after 7 days exposure of pyrite to 200 bar hydrogen at 120 °C.

Furthermore, it is noteworthy to mention that XRD analysis has magnetite identified as being present in the reacted powder after the control experiment with nitrogen, i.e., apparently some pyrite oxidation took place. More research is needed to provide a decisive answer if magnetite was actually formed and how, because the oxidation of pyrite to form magnetite is commonly known to only occur at much higher temperatures (Thorpe et al. 1987). In the presence of hydrogen this reaction is suppressed and therefore no magnetite is detected in the other samples. Truche et al. 2013 also detected magnetite in experiments at pH >10 for experiments with H_2, so at specific conditions the formation of magnetite is favourable.

As previously explained, for all conditions stated in Table 2, experiments are executed after 1, 3 and 7 days. Figure 11 shows the mol% of pyrite measured in the reacted powder against exposure time. At 120 and 150 °C a significant decreasing trend can be observed. At 80 °C though this trend is not observed, and in the qualitative experiment (Table 1, exp. D) pyrrhotite was not observed either, although it may be present below the XRD detection limit. A longer-duration experiment should be conducted to find out whether it occurs or not at this temperature, albeit at a slow rate.

Besides the temperature, the pressure (30 and 200 bar) and particle size (<40 and <5 micron) were also varied. The results of these experiments are plotted in Figure 12. It can be seen that there is a weak dependence of the conversion rate on pressure, i.e., a lower pressure results in less pyrite conversion. What mechanism is behind this pressure dependence can only be speculated on. It could be the effect of higher pressure itself which allows the hydrogen to penetrate deeper into the particle, or it could be the effect of pressure on solubility of hydrogen, i.e., at higher pressure more hydrogen is dissolved into the brine, and available for the reaction.

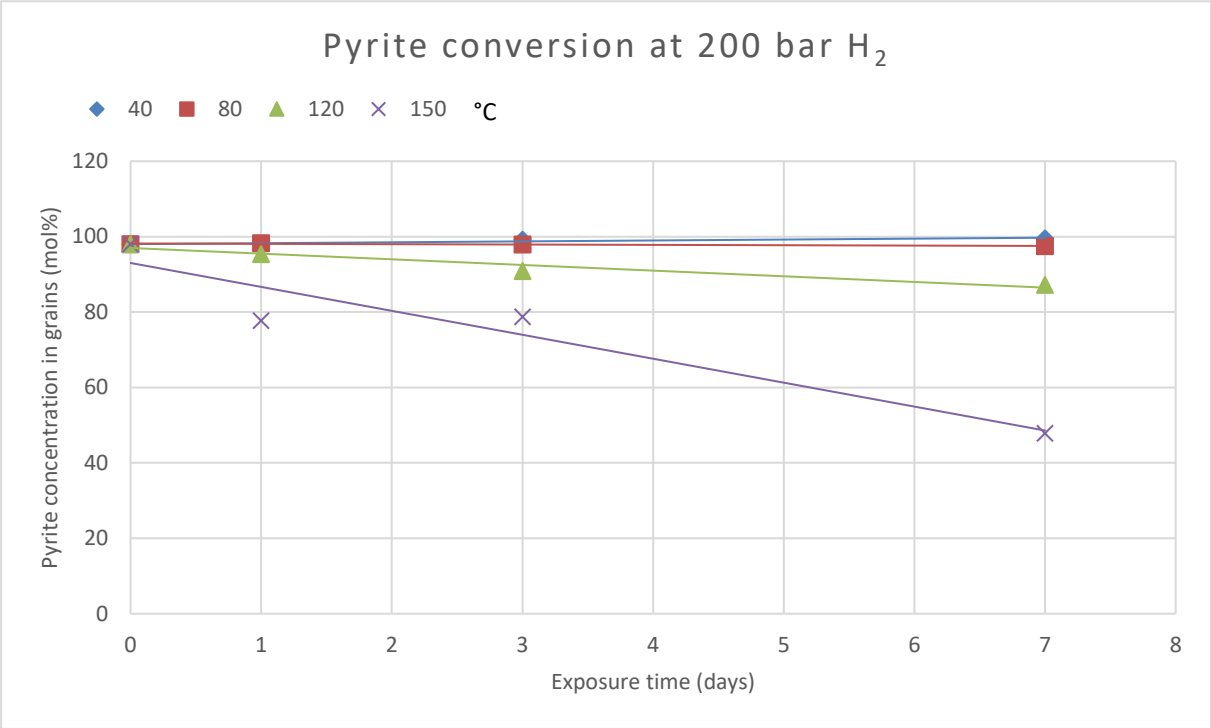

Figure 10. Pyrite reduction as function of exposure time, with different temperatures at 200 bar H2.

Likewise, the particle size (proxy for surface area) has a significant and more dramatic effect. Although the weighing amount in mass is the same for the experiments with <40 micron and <5 micron particles, the surface area exposed to hydrogen is much higher for the 5 micron particles, hence the reaction rate per gram is much higher too, as the reactivity directly corresponds to the amount of surface area available. In support of this statement, the results of the nitrogen gas adsorption analyses by Brunauer-Emmett-Teller (BET) method, indicates a surface area of 1.087 m^2/g for the <40 micron particles vs. 12.257 m^2/g for the <5 micron particles, i.e., 11 times more surface area is exposed for 5 micron particles than for <40 micron particles, which explains the difference in reaction rates observed. The reaction already slows down after one day as the reaction products such as Fe^{2+} and HS^- accumulate in the brine, the reaction reaches equilibrium and will slow down and ultimately stop reacting. In addition, the surface area has reacted to an increasing extent and is covered with the reaction product pyrrhotite. Pyrrhotite is lower in molecular volume, which would allow the hydrogen to still diffuse towards pyrite to some extent, yet the extent of reactivity is likely reduced.

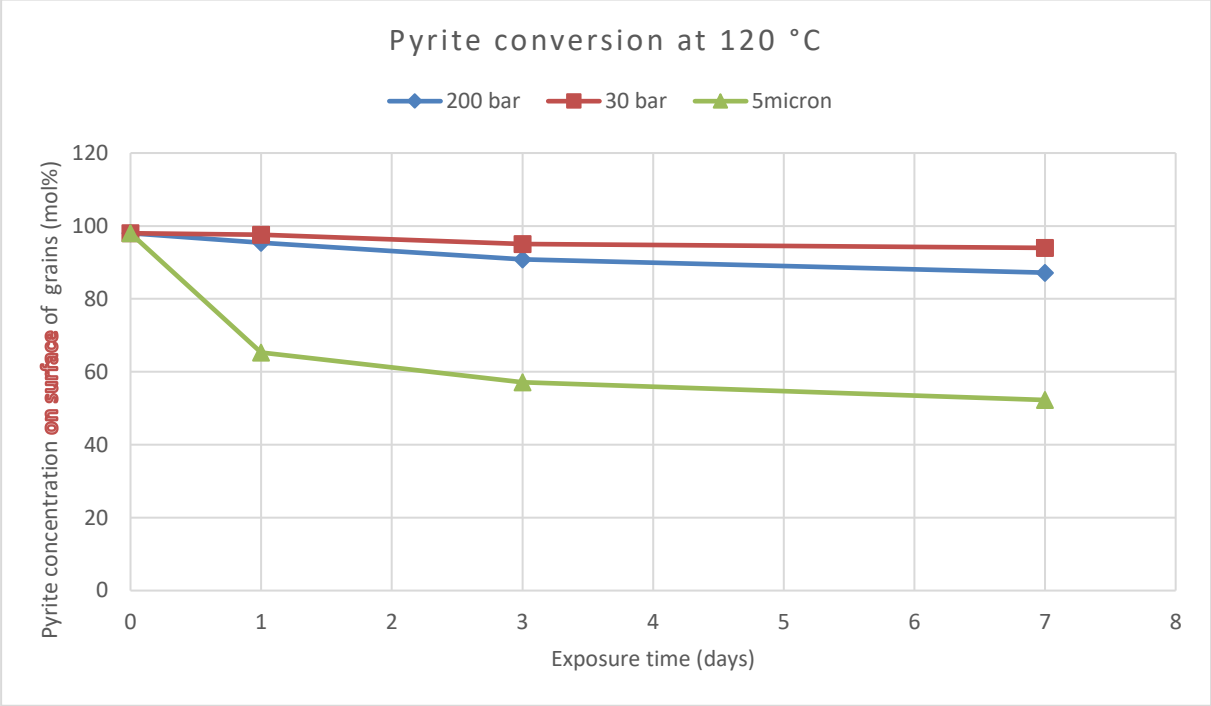

Figure 11. XRD results of reacted powder at 30 bar vs 200 bar and <5 micron particles vs <40 micron.

All pyrite reduction experiments are summarized in tables 4 and 5, which include the results of calculations made for total H_2S production and total H_2 loss after 1, 3 and 7 days (Table 4), based on the measured amounts of pyrite, pyrrhotite and troilite for all experiments after 1, 3 and 7 days exposure time (Table 5). With the assumption that one mole of reduced pyrite makes one mole H_2S, the production of H_2S in mg can be calculated. First, the amount of pyrite reduction in Table 4 is calculated as the wt% of the reacted powder divided by the amount of the virgin powder (Table 5). With this fraction the total amount of moles pyrite can be calculated as well as the amount of moles H_2S which are produced and therefore also the amount in mg. It must be noted that amounts calculated, assume that the pyrite particles -that the XRD identifies as (partly) pyrrhotite- are completely (homogeneously) converted i.e., that the hydrogen fully penetrated to the core of the particles. In reality, it is possible that the penetration depth was more limited, especially for the <40 microns particles, given that the estimated penetration depth of the XRD signal for pyrite crystals is in the order of 10 microns. Therefore, the actual amounts of H_2S produced in the experiments are probably somewhat lower than calculated.

Table 4. Results of pyrite reduction in stirred batch experiments.

Exp No	Size (µm)	P (bar)	T (°C)	Exposure time (days)	Pyrite reduction (wt%)	mg H_2S prod. per 0.5g FeS_2	mg H_2 loss per 0.5g FeS_2
9	<40	200	150	1	21%	29,4	1,7
				3	20%	27,9	1,7
				7	51%	72,7	4,3
9b, N_2	<40	200, N_2	150	7	6%	8,7	0,5
1a	<40	200	120	1	3%	3,8	0,2
				3	7%	10,3	0,6
				7	11%	15,7	0,9
4	<40	200	80	1	0%	0,0	0,0
				3	0%	0,1	0,0
				7	1%	0,7	0,0
2	<40	200	40	1	0%	0,1	0,0
				3	0%	0,0	0,0
				7	0%	0,0	0,0
3	<40	30	120	1	0%	0,7	0,0
				3	3%	4,2	0,2
				7	4%	5,8	0,3
5	<5	200	120	1	33%	47,3	2,8
				3	42%	59,3	3,5
				7	47%	66,3	3,9

Table 5. XRD Rietveld results of stirred batch experiments (TNO).

Exp No	Size (µm)	P (bar)	T (°C)	Exposure time (days)	Pyrite (wt%)	Pyrrhotite (wt%)	Troilite (wt%)	Magnetite (wt%)
0, virgin	<40	-	-	0	98,0	1,2		
9	<40	200	150	1	77,69	18,53	3,78	
				3	78,72	17,54	3,74	
				7	47,83	42,07	10,1	
9b, N_2	<40	200, N_2	150	7	92,03	2,50	0,10	5,37
1a	<40	200	120	1	95,40	4,46	0,14	
				3	90,86	7,99	1,15	
				7	87,19	11,51	1,30	
4	<40	200	80	1	98,26	1,68	0,07	
				3	97,94	2,00	0,05	
				7	97,49	2,39	0,13	
2	<40	200	40	1	97,95	2,05		
				3	99,20	0,79	0,01	
				7	99,55	0,32	0,13	
3	<40	30	120	1	97,55	2,29	0,16	
				3	95,09	3,59	1,32	
				7	93,99	5,01	1,00	
5	<5	200	120	1	65,33	31,14	3,53	
				3	57,11	39,85	3,04	
				7	52,27	44,87	2,86	

3.1.5 Stirred Batch Experiment Interpretation

Improved fundamental understanding of the hydrogen-driven reduction reaction of pyrite and its risks for UHS requires a) a set-up and protocols for conducting experiments under fully controlled conditions representative of subsurface reservoirs (anaerobic high pressures of hydrogen up to ~ 200 bars and temperatures up to ~ 120 °C), and b) a diverse set of measurement techniques to measure amounts of reaction products in the solid, liquid and gas phases inside the reactor during and/or after the experiment.

It proved to be very challenging to develop a fully HSE-compliant experimental set-up and protocol because of the rare combination of pressure, temperature, pH-range (pH 5-9), and specific gases (H_2, H_2S), which required special materials, components, and coatings, and to develop protocols for sample handling and working oxygen free. Furthermore, it took time to select the best techniques to monitor the reaction while ongoing and to analyse the reaction products post-mortem. In particular, sampling of the gas mixture from the reactor headspace for GC-MS analysis turned out the be very complicated for two reasons.

Firstly, it proved to be very challenging to take multiple gas samples at regular time intervals during the experiment without disturbing the reaction conditions (partial pressures, ratios of dissolved vs. free gases, in particular H_2S). Secondly, moisturized multi-component gas samples with H_2S proved to be hard to analyse correctly with GC-MS, partly due to condensation. The water condensate will dissolve H_2S which is therefore extracted from the gas in the sample, whereupon the GC-MS could give a false, too low, signal of H_2S. In the end, post-mortem analyses of the powder with XRD and Rietveld refinement turned out to be the most reliable method for accurately measuring the amount of conversion in the stirred batch experiments at TNO. For future experiments it would be beneficial to also analyse the liquid phase for e.g. dissolved iron and sulphur species as well as hydrogen sulphide.

The qualitative results obtained from the first series of experiments (where the headspace was sampled with GC-MS, and the solid with XRD but yet without Rietveld refinement) already proved that pyrite can reduce to form pyrrhotite-group mineral phases in the presence of hydrogen under subsurface P, T conditions, building on and confirming similar findings of Truche et al. (2009, 2010, 2013), who performed similar experiments at lower partial hydrogen pressures. SEM pictures show clear reacted surface of pyrite with grown crystals on top and EDX confirms a reduction of pyrite.

From the quantitative results of the second series of experiments we can derive how much pyrite is converted into pyrrhotite (and troilite), calculate how much H_2S must have formed, and to what extent the rate of conversion depends on pressure, temperature, grain size (surface area) and pH. The data clearly show that temperature has a big impact on the rate of pyrite reduction; where at 150 °C after 1 day already over 20% was reduced to pyrrhotite and troilite, at 80 °C after 7 days the amount of conversion was low, and not far above the initial pyrrhotite concentration in the virgin powder, i.e., the result was inconclusive. Moreover, with XRD no significant reduction of pyrite was observed at 80 °C, although an increase of pyrrhotite and a small amount of troilite is found by XRD Rietveld refinement, implying that the reaction could have been taking place, albeit at a low rate. An experiment with longer exposure time of one month at 80 °C could confirm if the reaction occurs or not.

Pressure also was found to influence the reaction rate, but much more mildly than temperature. While at 200 bar and 120 °C 13% conversion is measured, at 30 bar and similar temperature 6% conversion is measured. A hypothesis for this pressure effect is that at higher pressure more hydrogen can dissolve into the brine and is therefore available for the reaction (which

happens in the liquid phase) than at 30 bar. Also, the pressure itself may influence the reaction rate, by allowing the hydrogen to penetrate deeper into the pyrite.

The effect of available surface area is profound. While at 120 °C and 200 bar 13% conversion is measured when using particles up to 40 microns, 48% conversion is measured at the same conditions when using particles up to 5 micron, on which 11 times more surface area is exposed. It should be noted that for the freshly grinded particles of size < 5 micron, relatively more fresh and reactive surface is probably available than would be the case for natural pyrite, especially in geological reservoirs.

The effect of pH cannot be demonstrated on the basis of our experimental results. The qualitative results of the experiments B and C of the first series show both a conversion into pyrrhotite at pH 9 and pH 7. However, Truche et al. (2010, 2013) already showed that the reaction is pH-dependent at lower partial hydrogen pressures. To firmly establish to what extent pH affects the rate of the reaction at reservoir conditions, selected experiments should be repeated at a range of pH (pH 5-9).

To conclude, the results of the stirred batch experiments show that at temperatures of 120 °C and higher the conversion of pyrite to pyrrhotite is fast, which leads to the production of a stoichiometric amount of hydrogen sulphide. As an indication, the calculated (average) rate of H_2S production for the reference experiment (using the values after 1, 3, and 7 days for experiment #1a in Table 4) at a temperature of 120 °C, a pressure of 200 bar, a pH of 9 and particle size of <40 micron are in the order of 4-8 mg/day per gram of pyrite, accompanied by 0.2–0.4 mg/day of hydrogen loss, with the remark that the actual amount of H_2S produced was probably somewhat lower because the calculation assumes a homogeneous reaction rate over the whole pyrite particle. For the experiment at the same pressure, temperature and pH, but with particle size of < 5 microns (experiment #5 in Table 4), the calculated rates of H_2S production and H_2 loss are in the order of 19–95 mg/day and 1–6 mg/day respectively, per gram of pyrite, and with clear indication that the reaction rate decreases rapidly with time.

At 80 °C and lower, the rate of reaction is low, and longer duration exposure reactions are necessary to provide unequivocal evidence whether the reaction is slow or that there is no reaction at all.

3.2 Static batch experiments (University of Edinburgh)

3.2.1 Materials and Methods

Research-grade hydrogen (H_2) and nitrogen (N_2) gases (purity 99.9995 vol %) and sodium chloride (NaCl) of certified purity (99.5%) were supplied by BOC Ltd. and Fisher Scientific, respectively. Deionized water generated by an integral water purification system (ELGA DV 25) was used exclusively throughout the experiments. A relatively pure pyrite sample (specimen grade sample from Zacatecas, Mexico, supplied by Ward's Natural Science Establishment Inc.) was used for this work, along with a specimen grade calcite sample (also supplied by Ward's Science) and a sample of sandstone reservoir (sub-sampled from a core retrieved from the Rough Field, North Sea, and supplied by Centrica). For use in the experiments, samples were crushed and sieved to a <355 µm fraction. Gross sample mineralogy was determined by X-ray diffraction (Bruker D8 - Powder Diffractometer: scanning parameters 0−90°, 2θ, accuracy in peak positions ≤0.01 2θ, Bragg−Brentano configuration). Mineral phases were identified using the internal Bruker database with EVA analysis package.

Experiments were carried out in custom designed 316 stainless steel reaction vessels, made at the University of Edinburgh. For experimental runs, each vessel was stacked with a series of glass containers each holding 15 g of crushed rock sample (except for brine only control runs) and 50 g 3.5 wt% NaCl. Vessels were then sealed and placed in a fan oven (SciQuip Oven-110S). Following evacuation (to remove free oxygen), using a CPS VP2S pro-set single-stage vacuum pump, vessels were pressurised with either H_2 or N_2. During runs vessel pressure and temperature conditions were measured continuously using a GD4200-US Digital Pressure Transducer from Elemental Science Inc. Data were recorded on a PC at 1 min intervals; the measurement errors for pressure and temperature were quantified as < ±0.15% span best fit straight line and ±1.5%FS total band, respectively.

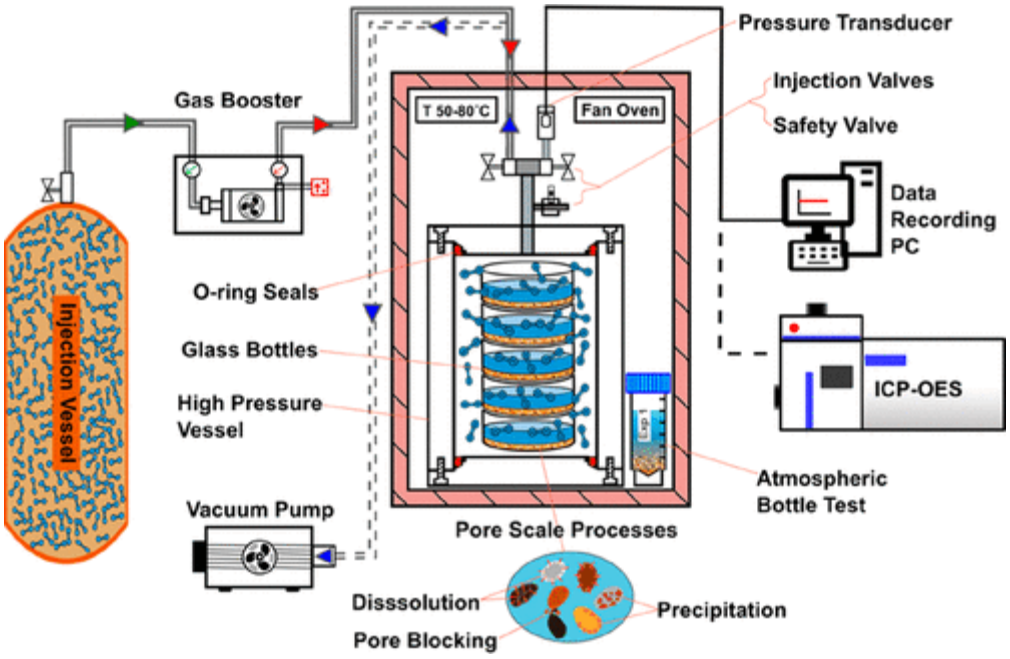

Figure 12. Experimental apparatus. Schematic diagram of static batch reactor setup.

Experimental runs were carried out at 80℃ and at a target/starting pressure of 60 bar. Note that due to leakage over time the average pressure during some runs fell below this target (see Table 2). All runs lasted for a duration of 68 days, at the end of which vessels were depressurised and a liquid sample retrieved from each of the glass containers and filtered through a 0.2 µm nylon filter at which point a split was taken and acidified for ICP-OES analysis. Measurements of pH and conductivity were made on the filtered samples and compositional analysis carried out via inductively coupled plasma−optical emission spectroscopy (ICP-OES) using a Varian Vista Pro with APEX-E from Elemental Science Inc. (LoD of 0.105 × 103 to 0.26 ppm or ~ 0.2−100 ppb). After the vessels were evacuated using a CPS VP2S pro-set single-stage vacuum pump, H_2 and N_2 gas were introduced from their respective cylinders through a valve at the top of the vessel. Vessel pressure and temperature conditions were measured continuously using an 1–1000 bar ESI pressure transducer.

3.2.2 Static Batch Experiment Results

3.2.2.1 Experiments with pure pyrite

Experiments carried out using pyrite samples (either sedimentary pyrite or a specimen grade 'pure' pyrite) are summarised in Table 6. These experiments were carried out using a specimen grade pyrite sample. The specimen sample pyrite was found to be 100% pyrite as determined by XRD.

Five experiments were carried out using the specimen pyrite using hydrogen as the pressurizing medium. These comprised one run at c. 206 bar pH_2 and 80℃, one run and one duplicate run at c. 124 bar pH_2 and 80℃ and one run and one duplicate run at approx. 103 bar pH_2 and 120℃. For each set of conditions control runs using N_2 rather than H_2 as the pressurizing medium were also undertaken. Select analytical results for these runs are presented in Table 7 and Figure 13, while full analytical results can be found in Section 6.

Both nitrogen and hydrogen runs are characterised by elevated sulphur and iron concentrations and low pH which ranges from c. 5.6 to 2.0 in the runs presented here. These parameters also show a strong correlation with temperature (higher temperature runs showing increased Fe and S concentrations and lower pH. Dependence on pressure is uncertain: run pairs 1081/1102 and 1088/1107 should provide a direct comparison of pressure effects, but the Fe and S concentrations reported for run 1081 are suspect, being very low compared to other runs and are likely the result of a sample handling/labelling issue.

The release of Fe and S to solution is clearly an indicator that pyrite dissolution is taking place in these systems. It is notable that the dissolution in these runs show little to no dependence on the presence of H_2. Comparison between H_2/N_2 run pairs 1102/1115, 1134/1136, and 1146/1149 shows that Fe concentrations for hydrogen runs are within ±16% of those reported for their comparative nitrogen runs. Sulphur concentrations show a wider discrepancy: they are consistently lower in hydrogen runs, relative to the nitrogen runs, but the difference is, at most, around 22% and likely within experimental error. Aside from run 1081, molar ratios between Fe and S range between 0.65 and 0.22, with a mean value across all runs of 0.41. There is little difference between these values for H_2/N_2 run pairs.

While it was not possible to undertake any analytical work on the post reaction solids the formation of a yellow, secondary precipitate on the surface of the solids retrieved from runs 1146 and 1149 was noted. This may be elemental sulphur, or possibly an iron bearing phase (i.e. siderite) and was observed in a number of the experiments carried out at 120℃. The conditions for these runs lies very slightly above the melting point for elemental sulphur and

we therefor believe it likely that, if they are indeed sulphur, these precipitates did not form in-situ, but during cooling and depressurisation.

Table 6. Summary of experiments using pyrite samples.

Run ID	Solid	Solid Type	Solid Weight (g)	Temperature (°C)	Average Pressure (bar)	Gas	Starting fluid	Fluid weight (g)	Run Time (days)	End pH	End conductivity (µs/cm)
1081	AGH0020	Pyrite	15	80	206	H2	3.5% NaCl	50	14	3.924	NM
1088	AGH0020	Pyrite	15	80	206	N2	3.5% NaCl	50	14	3.723	NM
1102	AGH0020	Pyrite	15	80	124	H2	3.5% NaCl	50	14	5.55	NM
1107	AGH0020	Pyrite	15	80	124	H2	3.5% NaCl	50	14	5.157	NM
1115	AGH0020	Pyrite	15	80	124	N2	3.5% NaCl	50	14	4.898	NM
1134	AGH0020	Pyrite	15	120	103	H2	3.5% NaCl	50	14	3.651	58609
1136	AGH0020	Pyrite	15	120	103	N2	3.5% NaCl	50	14	2.068	65210.5
1146	AGH0020	Pyrite	15	120	103	H2	3.5% NaCl	50	14	2.192	64811
1149	AGH0020	Pyrite	15	120	103	N2	3.5% NaCl	50	14	2.002	6480.6

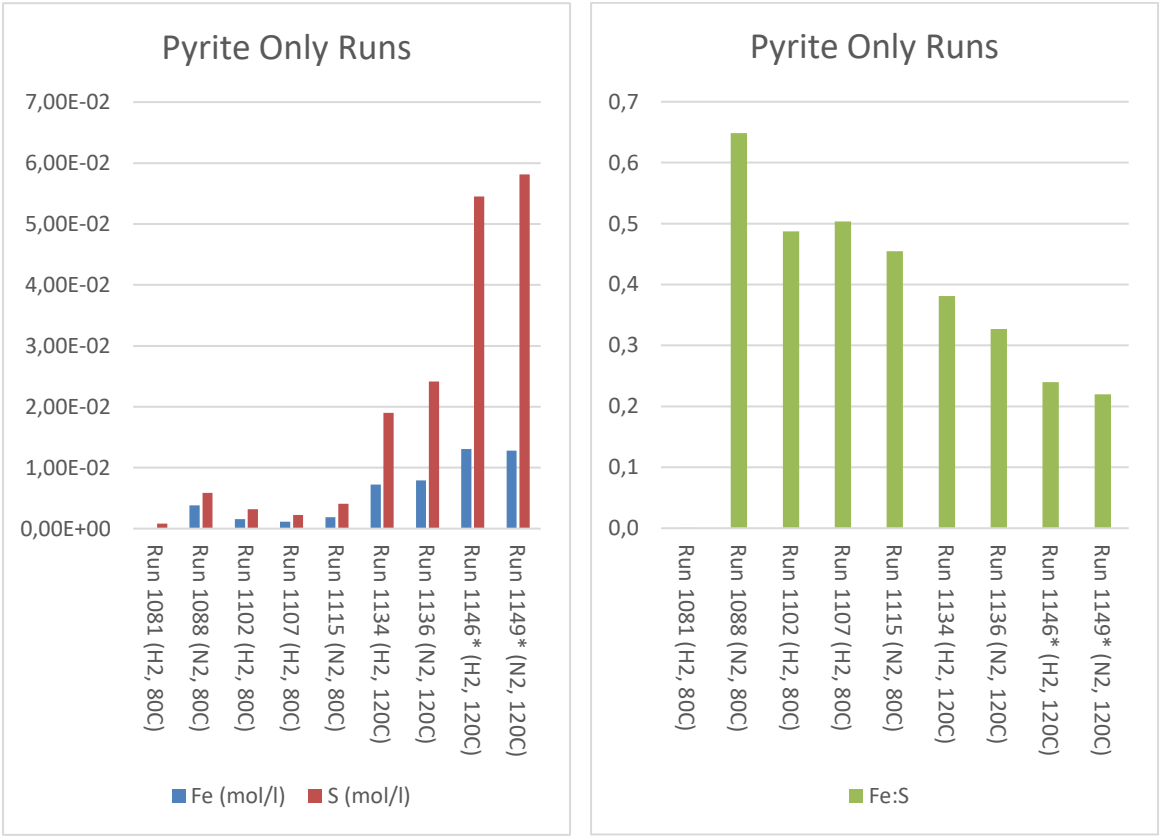

Figure 13. Charts of select results from pyrite only runs.

Run	1081		1088		1102		1107		1115		1134		1136		1146*		1149*	
Solid	AGH0020		AGH0020		AGH0020		AGH0020		AGH0020		AGH0020		AGH0020		AGH0020		AGH0020	
Sample type	Pyrite		Pyrite		Pyrite		Pyrite		Pyrite		Pyrite		Pyrite		Pyrite		Pyrite	
Run time (days)	14		14		14		14		14		14		14		14		14	
Run temp. (℃)	80		80		80		80		80		120		120		120		120	
Run Pressure (bar)	206		206		124		124		124		103		103		103		103	
Gas	H2		N2		H2		H2		N2		H2		N2		H2		N2	
End pH	3.924		3.723		5.55		5.157		4.898		3.651		2.068		2.192		2.002	
End conductivity (us/cm)	NM		NM		NM		NM		NM		58609		65210.5		64811		6480.6	
Element	ppm	mol/l	ppm	mol/l	ppm	mol/l	ppm	mol/l	ppm	mol/l	ppm	mol/l	ppm	mol/l	ppm	mol/l	ppm	mol/l
Fe	*0.011⁺*	*1.92E-07*	*211.896*	*3.79E-03*	*86.967*	*1.56E-03*	*62.772*	*1.12E-03*	*103.100*	*1.85E-03*	*404.442*	*7.24E-03*	*441.368*	*7.90E-03*	*730.164*	*1.31E-02*	*713.392*	*1.28E-02*
S	*26.048⁺*	*8.12E-04*	*187.546*	*5.85E-03*	*102.525*	*3.20E-03*	*71.581*	*2.23E-03*	*130.138*	*4.06E-03*	*609.712*	*1.90E-02*	*774.793*	*2.42E-02*	*1747.960*	*5.45E-02*	*1863.316*	*5.81E-02*
Fe:S		*0.0002*		*0.6487*		*0.4870*		*0.5035*		*0.4549*		*0.3809*		*0.3271*		*0.2398*		*0.2198*

Table 7. Select results for runs using pyrite only

*(⁺unusually low concentrations marked may represent a sample handling issue, *runs where significant quantities of yellow precipitate observed).*

3.2.2.2 Experiments with mixture of pure pyrite and calcite

Previous work has identified that the reduction of pyrite in the presence of hydrogen can occur in systems where solution pH is buffered by calcite, albeit at higher temperature than those used in this work (Truche et al. 2010). Therefore the experimental procedure described above was repeated utilizing calcite as a buffering agent mixed with the starting pyrite in various proportions. The calcite utilized in these runs was a specimen grade calcite sample supplied by Ward's Sciences. The experiments undertaken in this manner are summarized in Table 8.

These experiments comprised two runs using hydrogen as the pressurizing medium: one using a 50:50 mixture of pyrite and calcite as the starting solid and one using a 99:01 mixture of pyrite and calcite. The conditions of these runs were duplicated in two control runs using nitrogen, rather than hydrogen, as the pressurising medium.

Table 8. Summary of experiments carried out using pyrite and calcite.

Run ID	Solid	Solid Type	Solid Weight (g)	Temperature (°C)	Average Pressure (bar)	Gas	Starting fluid	Fluid weight (g)	Run Time (days)	End pH	End conductivity (µs/cm)
1140	AGH0020+AGH0023	Pyrite + 50% Calcite	15	120	103	H2	3.5% NaCl	50	14	7.307	61288.3
1142	AGH0020+AGH0023	Pyrite + 50% Calcite	15	120	103	N2	3.5% NaCl	50	14	7.436	61565.2
1148	AGH0020+AGH0023	Pyrite 99% + 1% Calcite	15	120	103	H2	3.5% NaCl	50	14	2.225	64092.2
1151	AGH0020+AGH0023	Pyrite 99% + 1% Calcite	15	120	103	N2	3.5% NaCl	50	14	1.462	71135.2

Select analytes, measured at the end of these runs, are presented in Table 9 and Figure 14 (along with the results from a calcite free equivalent run, for comparison), while full chemical analyses are presented in Section 6.

As for the pyrite only runs, the results for experiments using pyrite-calcite mixtures indicate that the presence of hydrogen has relatively little influence on the dissolution of pyrite observed, with elemental concentrations and pH are closely comparable between the H_2/N_2 run pairs.

The runs containing 1% calcite have, like the pyrite only experiments, notably depressed pH. Indeed run 1151 has a pH (1.5) lower than any observed in the pyrite only runs. Similarly, Fe and S concentrations in these runs are notably higher than those observed in the pyrite only runs.

*Table 9. Select results for Pyrite-Calcite experiments (*runs where substantial quantities of yellow precipitate was observed).*

Run	1140		1142		1148*		1151*		1134	
Solid	AGH0020+AGH0023		AGH0020+AGH0023		AGH0020+AGH0023		AGH0020+AGH0023		AGH0020	
Sample type	Pyrite + 50% Calcite		Pyrite + 50% Calcite		Pyrite 99% + 1% Calcite		Pyrite 99% + 1% Calcite		Pyrite	
Run time (days)	14		14		14		14		14	
Run temp. (℃)	120		120		120		120		120	
Run Pressure (bar)	103		103		103		103		103	
Gas	H2		N2		H2		N2		H2	
End pH	7.307		7.436		2.225		1.462		3.651	
End conductivity (us/cm)	61288.3		61565.2		64092.2		71135.2		58609	
Element	ppm	mol/l	ppm	mol/l	ppm	mol/l	ppm	mol/l	ppm	mol/l
Ca	*444.680*	*1.11E-02*	*433.726*	*1.08E-02*	*170.565*	*4.26E-03*	*177.756*	*4.44E-03*	*14.757*	*3.68E-04*
Fe	*0.216*	*3.87E-06*	*0.158*	*2.83E-06*	*859.932*	*1.54E-02*	*834.515*	*1.49E-02*	*404.442*	*7.24E-03*
S	*722.525*	*2.25E-02*	*707.283*	*2.21E-02*	*4542.189*	*1.42E-01*	*4338.039*	*1.35E-01*	*609.712*	*1.90E-02*
Fe:S		*0.0002*		*0.0001*		*0.1087*		*0.1105*		*0.3809*

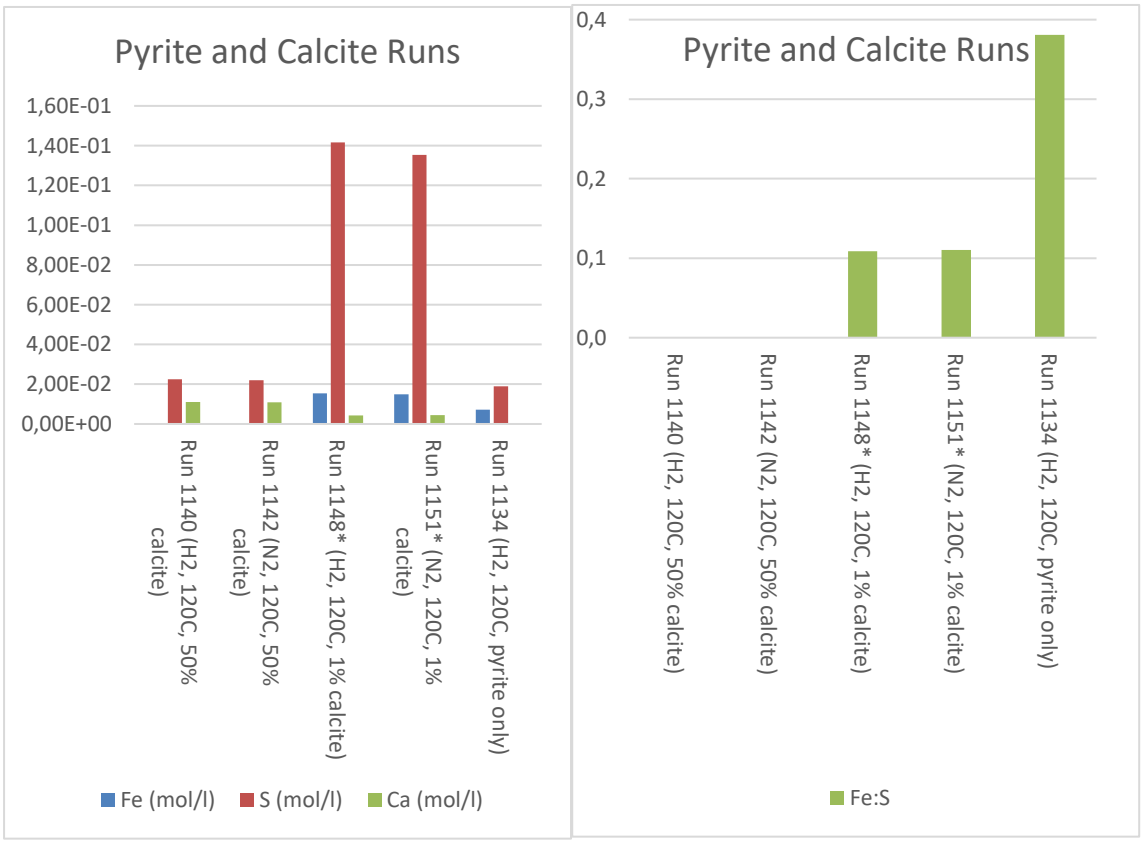

Figure 14: Charts of select results from pyrite-calcite runs.

The results are markedly different for the runs using 50% calcite. Here pH is high (7.3-7.4), relative to the other pyrite experiments undertaken, at the end of the runs. As might be expected Ca concentrations are higher in these runs, relative to their 1% calcite counterparts,

but Fe concentrations are very low (<1 ppm) while S concentrations are elevated, but low relative to those observed in the 1% calcite runs. The results indicate that pH remains relatively well buffered in the 50% mixture experiments, but relatively unbuffered in the 1% calcite experiments. The Ca concentrations, however, do not suggest that all of the calcite is dissolved. This is indicative of a stirring issue, i.e., all *available* calcite in the 1% calcite runs is dissolved, thereafter allowing pH to fall, but there remains a substantial proportion of the calcite in the powdered sample which is simply unavailable to the fluid for reaction.

The Fe-S ratios for the runs containing calcite are also notably different to the pure pyrite runs. In all cases they are lower: slightly lower, in the case of the 1% calcite runs (0.1 vs 0.4 for the comparative pyrite only run) and considerably (around three orders of magnitude) lower in the case of the 50% calcite runs. As for the pyrite only runs carried out at 120°C, a yellow precipitate was noted for two of these runs. Notably this precipitate was not observed for the two runs containing 50% calcite.

3.2.2.3 Experiments with mixture of pure pyrite and reservoir sample

In addition to the experiments carried out using the pyrite and calcite samples described in the previous section, experiments were also carried out using a reservoir sample (sub-sampled from a core retrieved from a field in the North Sea, UK) mixed with varying amounts of the 'pure' specimen grade pyrite, in order to observe the reaction of pyrite as part of a more representative mineral assemblage. The results of XRD analysis of the reservoir sample used are presented in Table 10, while Table 11 summarises the experiments undertaken. The experiments comprised three runs using hydrogen as the pressurizing medium: one using the reservoir sample only, one using a mixture of reservoir sample and 10% pyrite and one using the reservoir sample and 20% pyrite, together with equivalent control experiments using N_2 as the pressurizing medium.

Select analytes for these experiments are presented in Table 12 and Figure 15, while full analytical results can be found in Section 6.

Table 10. XRD analysis of the reservoir sample used.

Phase	AGH0007
Quartz	78.75
Calcite	ND
Dolomite	4
Albite	1.48
Pyrite	0.03
Gypsum	0.08
Illite	1.63
Orthoclase	1.46
Microcline	4.71
Na-Ca-Feldspar	2.89
Kaolinite	1.26
Muscovite	1.59
Chamosite	0.56
Chlorite	1.56
Barite	ND
Montmorillonite	ND

Table 11. Summary of experimental runs undertaken using pyrite and reservoir samples.

Run ID	Solid	Solid Type	Solid Weight (g)	Temperature (°C)	Average Pressure (bar)	Gas	Starting fluid	Fluid weight (g)	Run Time (days)	End pH	End conductivity (µs/cm)
1109	AGH0007	Res. sample	15	80	124	H2	3.5% NaCl	50	14	9.149	NM
1117	AGH0007	Res. sample	15	80	124	N2	3.5% NaCl	50	14	9.409	NM
1111	AGH0007+ AGH0020	Res. sample + 10% Pyrite	15	80	124	H2	3.5% NaCl	50	14	9.526	NM
1112	AGH0007+ AGH0020	Res. sample + 20% Pyrite	15	80	124	H2	3.5% NaCl	50	14	9.537	NM
1119	AGH0007+ AGH0020	Res. sample + 10% Pyrite	15	80	124	N2	3.5% NaCl	50	14	9.377	NM
1120	AGH0007+ AGH0020	F + 20% Pyrite	15	80	124	N2	3.5% NaCl	50	14	9.389	NM

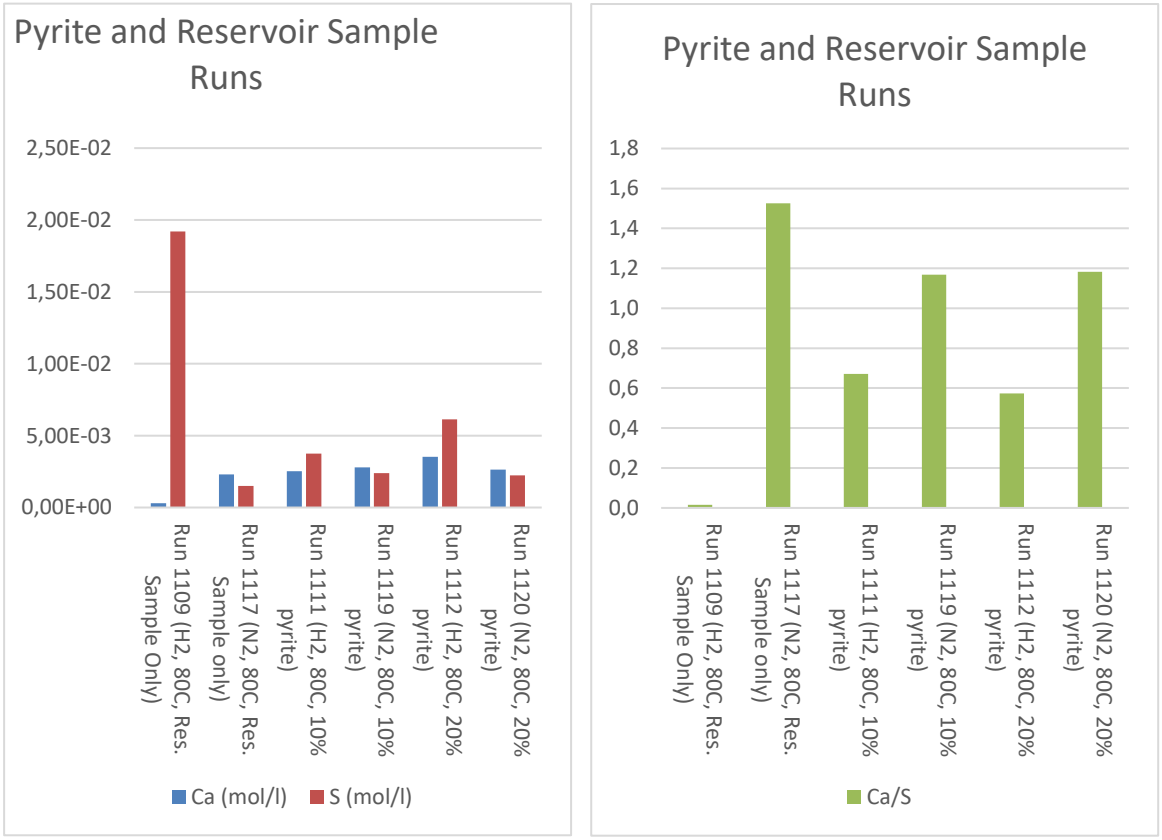

Figure 15. Charts of select results from runs using reservoir samples and pyrite.

Table 12. Select analytes from reservoir sample-pyrite experiments.

Run	1109		1117		1111		1119		1112		1120	
Solid	AGH0007		AGH0007		AGH0007+AGH0020		AGH0007+AGH0020		AGH0007+AGH0020		AGH0007+AGH0020	
Sample type	Res. sample		Res. sample		Res. sample + 10% Pyrite		Res. sample + 10% Pyrite		Res. sample + 20% Pyrite		Res. sample + 20% Pyrite	
Run time (days)	14		14		14		14		14		14	
Run temp. (℃)	80		80		80		80		80		80	
Run Pressure (bar)	124		124		124		124		124		124	
Gas	H2		N2		H2		N2		H2		N2	
End pH	9.149		9.409		9.526		9.377		9.537		9.389	
End conductivity (us/cm)	NM		NM		NM		NM		NM		NM	
Element	ppm	mol/l	ppm	mol/l	ppm	mol/l	ppm	mol/l	ppm	mol/l	ppm	mol/l
Fe	*BD*	*BD*	*BD*	*BD*	*BD*	*BD*	*BD*	*BD*	*BD*	*BD*	*BD*	*BD*
S	*615.844*	*1.92E-02*	*48.441*	*1.51E-03*	*120.348*	*3.75E-03*	*76.523*	*2.39E-03*	*196.859*	*6.14E-03*	*71.603*	*2.23E-03*
Ca	*12.228*	*3.05E-04*	*92.379*	*2.30E-03*	*100.860*	*2.52E-03*	*111.744*	*2.79E-03*	*141.086*	*3.52E-03*	*105.885*	*2.64E-03*
Ca:S	-	*0.02*	-	*1.53*	-	*0.67*	-	*1.17*	-	*0.57*	-	*1.18*

For all runs using the reservoir material end run pH is high (>9.0) compared to the pyrite only or pyrite-calcite runs described in previous sections. Fe was not detected in any of the runs, while S shows both highest and lowest concentrations in the runs where no pyrite was added (616 ppm in the hydrogen run and 48 ppm in the nitrogen control run). Dissolved S concentrations are notably lower in the nitrogen control runs compared to their hydrogen counterparts.

The results indicate that dissolution of the primary mineral assemblage, with or without the presence of hydrogen, is a large source of dissolved S. It is possible that the primary source of this sulphur is the gypsum present, or potentially residuals from the drilling mud in recovered samples. Gypsum is moderately soluble in water. If gypsum dissolution is the primary source of sulphur in the experiments (rather than pyrite) then we would expect the molar concentrations of S and Ca to be similar. This is largely the case other than for the hydrogen run using no additional pyrite, where the Ca:S ratio is very low. This may be indicative of an erroneous result for S (which is notably elevated in this run) or of possible secondary precipitation of, e.g., a carbonate mineral. Otherwise, Ca:S ratios are near unity. The nitrogen control runs show Ca:S ratios slightly above unity, while the hydrogen runs have ratios slightly below unity. With the available data the reasons for this are ambiguous, but may be indicative of enhanced sulphur release under reducing conditions (i.e., from reduction of pyrite).

3.2.3 Static Batch Experiment Interpretation

Fuller interpretation of the results from the static batch experiments is hampered somewhat by lack of some key analytical data. These include Eh measurements on the reacted fluids, analysis for key redox-related species (HS^-, H_2S, SO_4^{2-}, Fe^{2+}, Fe^{3+}) and full analysis of the reacted and unreacted solids (SEM and XRD). These measurements were not made in the case of the static experiments due to time and facility constraints. Nevertheless, the experiments have provided a number of useful observations and a sound basis for further work in this area.

Runs carried out using pyrite only or pyrite-calcite mixtures showed evidence for dissolution of pyrite with notably elevated iron and sulphur concentrations in all runs. It is important to note that in all of these runs the presence of hydrogen made little difference to the results in terms of pH or Fe/S concentrations in solution. This indicates that dissolution in these experiments is not being caused by the reductive action of hydrogen, but through other mechanisms. Indeed, if dissolution were occurring purely through reduction (of the form presented in Equation 3.2.1a), then we would expect less release of iron to solution relative to sulphur (Fe:S 1:2). If sufficient Fe and S accumulated, FeS will form and the reaction will be traced only through additional release of sulphur and subsequent formation of H_2S (of the form presented in Equation 3.2.1b). In the case of these experiments significant iron is released, again suggesting, along with the low pH observed in several runs, other mechanisms at work.

$$FeS2 + H2 \rightarrow \ 〚Fe〛\hat{}(2+) + 2HS - \ (3.2.1a)$$

$$FeS_2 + H_2 \rightarrow FeS + H_2S \ (3.2.1b)$$

Oxidative dissolution, of the form presented in Equation 3.2.2, is one possible mechanism for this dissolution. This is supported by the low pH observed in the pyrite and pyrite/calcite runs, by the presence of significant concentrations of iron in solution and by the molar Fe:S ratios for the pyrite only runs, which tend to around 0.5. As shown in Equation 3.2.2 oxidative dissolution of pyrite, if proceeding stoichiometrically, would lead to release of one mole of Fe to every two moles of S. This observation does not hold true, however, for the experiments carried out using calcite/pyrite mixtures, where the molar ratios are somewhat lower. We suggest that the reason for this is the removal of released iron from solution, likely through precipitation of an iron carbonate phase (i.e., siderite, $FeCO_3$) and/or precipitation of iron oxyhydroxides as Fe is not soluble under oxidizing conditions at pH above 2-3, although we were not able to undertake analysis of the reacted solids to confirm this.

$$FeS_2 + 3.5O_2 + H_2O \rightarrow Fe^{2+} + 2SO_4^{2-} + H^+ \ (3.2.2)$$

While steps were taken to remove oxygen from the systems, via vacuum degassing and subsequent flushing of vessel headspace with nitrogen, the above observations suggest that these steps were not sufficient in removing free oxygen from the experimental systems for them to be reducing for the duration of the runs. However, as Equation 3.2.2 proceeds and free oxygen is consumed, it is possible that the experimental systems entered more reducing conditions later in the runs. Such conditions could also have led, eventually, to reductive dissolution of pyrite and subsequent formation of H_2S, though the only evidence for this occurring are the relatively low Fe:S ratios in the pyrite only runs where possible elemental sulphur was observed (the 120°C runs 1146 and 1149). These low ratios may suggest non-stoichiometric release of sulphur from the pyrite, though could also reflect loss of Fe from the system as a secondary precipitate.

In terms of the runs carried out using reservoir samples, lacking post-reaction analysis of the solids, there is little evidence that pyrite dissolution is occurring at all. If it is, it is likely also through oxidative, rather than reductive, dissolution, primarily, with any acidity generated being buffered via dissolution of primary minerals and any iron released being removed as secondary carbonate. It was notable, however, that these were the only experiments where the presence of hydrogen had a clear effect (slightly lower Ca:S ratios relative to the nitrogen control experiments). As for the pyrite only runs with low Fe:S ratios, it is possible that this is indicative of enhanced (relative to iron) sulphur release through reductive dissolution of pyrite at higher temperature (120°C) conditions.

When considering implications for “real-world” hydrogen storage operations it is important to bear in mind the limitations of the experimental system under consideration. While undertaken at pressure and temperature conditions relevant to geological storage of hydrogen all experiments began under far from equilibrium conditions. The majority of reaction which was observed was driven by disequilibrium between the NaCl brine used and the solid samples (as evidenced by the similarity in results between the hydrogen and nitrogen runs). Moreover a fine (<355 µm) fraction was used for these runs which will have included ultrafine material. This has the benefit of increasing reaction rates, making changes observable on reasonable timescales, but rapid dissolution of ultrafine material (which likely accounts for the majority of dissolved concentrations in these experiments) can drive dissolved concentrations far past mineral saturation points and is often not representative of how rocks/minerals will react in real systems. In a real-world, system changes if any, are likely to be more subtle: hydrogen will injected into systems which are likely at or close to equilibrium, in terms of the brine-rock chemistry. Further, while there is reasonable evidence that the experimental systems used were, initially at least, under oxygenating conditions, likely becoming more reducing as the experiments progressed, the majority of hydrogen storage sites will likely be reducing environments prior to injection of hydrogen. This is to say that the large changes induced in these experiments by inherent system disequilibrium may well mask more subtle changes which may be important in their real-world counterparts.

Hence, we can conclude that the introduction of hydrogen had little *observed* impact in the experiments presented here. While dissolution of pyrite was observed, the majority of dissolution was not driven by the presence of hydrogen. Notably there were a few experiments where there was some evidence for reductive dissolution of pyrite (where Fe:S or Ca:S ratios were notably low). We were not able to confirm this through direct observation of the reacted solids or analysis for H_2S.

4 Discussion, Conclusions, and Recommendations

The experiments presented here, as a whole, provide compelling evidence that reduction of pyrite in a hydrogen rich environment can be extensive and rapid at higher (>100°C) temperatures. This is particularly clear in the stirred batch experiments, presented in Section 3.2, where extensive (>10% at 120°C, and >50% at 150°C) conversion of pyrite to pyrrhotite (both in-situ and as a secondary precipitate) was observed together with generation of H_2S after a period of only seven days. The data from the static experiments is more ambiguous but does show some evidence (via Fe:S and Ca:S ratios) that reductive dissolution of pyrite occurred at 120°C. Static (unstirred) experiments carried out at temperatures below 120°C did not show any evidence for pyrrhotite formation but the stirred runs did show some evidence for the formation of troilite, another iron sulphide mineral and possible precursor to pyrrhotite. This suggests that the reaction is ongoing at these temperatures, albeit at a much-reduced rate.

These findings are of significance in terms of geological storage of hydrogen. Many hydrogen storage sites are likely to be within sedimentary basins, where pyrite is a common, albeit minor, mineral component. The formation of pyrrhotite itself may be a concern, in terms of modification to flow pathways and bulk reservoir permeability, but the primary concern will be the secondary formation of H_2S that pyrite reduction leads to. As well as resulting in a (small) net loss of hydrogen and contaminating the stored gas, H_2S may pose a risk to surface, as well as downhole, infrastructure, due to its corrosive nature and may be a cause for environmental or health concerns. It is useful, therefore, to consider the experiments presented here in the bigger picture of field-scale storage. In terms of temperature, the results presented here suggest that reduction of pyrite may be of primary concern only for higher temperature reservoirs (>80°C). There is evidence, however, that this reaction was occurring at 80°C, which raises the question of what the lower temperature limit is for this reaction to occur. The timescale of the experiments was a matter of days, while field scale storage will take place on timescales of months to years. Figure 16 indicates the temperatures encountered across the range of underground gas storage sites, shortlisted as suitable for hydrogen storage in HyUSPRe deliverable 1.5 (Cavanagh et al. 2023). As shown most are below 80°C. There is a need, therefore, to carry out lower temperature (60–100°C) experiments over a longer timescale to quantify this reaction, if it is occurring, for the lower temperatures and longer timescales more relevant to field scale storage. It is worth noting, however, that at the lower temperatures representative of many potential storage sites (<80°C), microbially mediated reactions would likely play a larger role in H_2 consumption and H_2S generation than the abiotic mechanism discussed here.

In terms of the overall magnitude and rate of this reaction, again the field-scale context should be borne in mind when considering the results presented here. The stirred experiments demonstrate that the reaction can be extensive in well stirred, high fluid:rock ratio systems. Here pyrite is ubiquitous and a large surface area is available to the fluid for reaction. At the field-scale pyrite will only be a minor (generally <5%) constituent of the overall reservoir mineralogy, surface area available for reaction will be lower, and will generally be less reactive than the fresh surfaces produced by grinding samples for experiments. Fluid:rock ratios will be considerably lower and, depending on the hydrodynamics of the system, pyrite surfaces may see relatively little hydrogen-charged fluids, which may equilibrate with the host rock relatively quickly, thereby retarding further reaction. This is not to say that the reaction will have little impact at the field scale, but that further work is required to upscale and quantify the potential impact of the results presented here at the field scale.

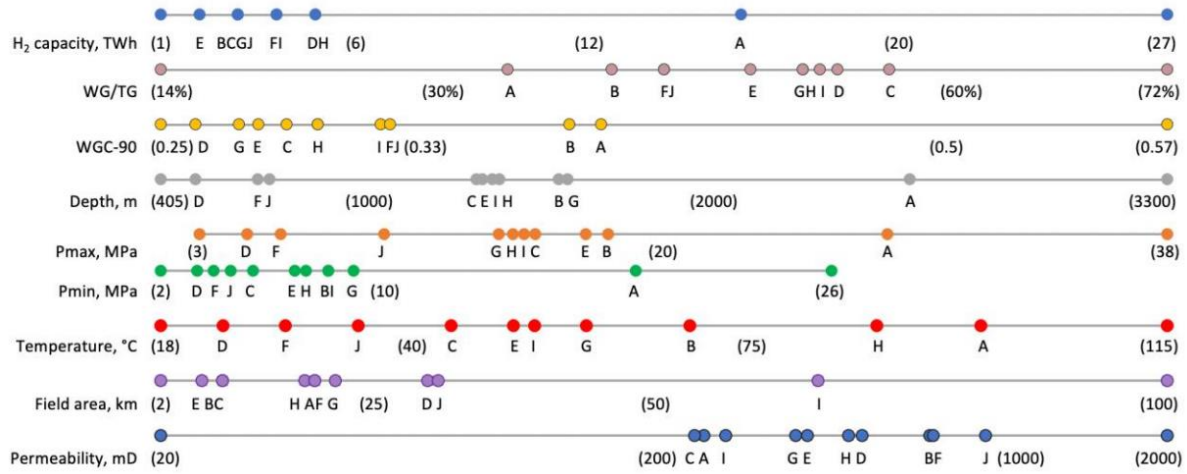

Figure 16. Data spread (including temperature, in red) for the shortlisted HyUSPRe underground gas storage sites across Europe, from HyUSPRe D1.5. Letters A-J are geographic identifiers, see full report for details.

Our recommendations as an extension to this work would therefore be for an experimental program focused on fully extrapolating the true rates of these reactions across a range of relevant temperatures, together with experiments more closely simulating the reservoir environment (i.e., flow-through experiments utilising reservoir cores or packed columns), coupled with reservoir scale reactive transport modelling to more fully quantify the likely impacts. If the H_2S concentration can be predicted by experiment-based models, adequate action can be taken to select proper materials and make decisions for facility design.

As a maximal case, in terms of H_2 consumption and H_2S generation we can consider the theoretical reaction only. Here, based on the molar mass of the reactants and products, 1 g of pyrite is reduced to 0.73 g pyrrhotite, releasing 0.27 g S. This S, in turn, can react to form 0.28 g H_2S, consuming 0.017 g hydrogen. If we extrapolate this to a theoretical mass of reservoir containing 1% pyrite, assuming that *all* pyrite is available for reaction with fresh, hydrogen charged fluid and a nominal porosity and density of 20% and 2000 kg/m^3, respectively, then we find that the pyrite in a 1 m^3 volume of reservoir has the potential to react with 0.34 g H_2, forming 5.7 g H_2S. This calculation may be of academic interest and does produce an upper bound for possible pyrite reaction but is clearly unrealistic in terms of an actual reservoir. Not all pyrite surface will be available for reaction, not all of the surface that is available will see hydrogen charged fluid and where the reaction does proceed it will become inhibited as equilibrium is approached and as available reactive surface area is reduced.

The stirred experiments presented here may, therefore, provide more realistic values for overall hydrogen consumption and H_2S production. In the experiment where maximum reactivity was observed (carried out at 150°C and 200 bar pH_2) 51% of the pyrite in the experiment was reduced to pyrrhotite over the course of seven days. Calculations based on the results from this experiment (see Section 3.1.5) indicate that this would equate to consumption of 0.0086 g of hydrogen for every gram of pyrite and generation of 0.15 g H_2S (i.e. 51% of the values from our theoretical, maximal, calculation). For our theoretical reservoir, this would equate to 0.17 g of hydrogen lost and 2.9 g H_2S generated for every square metre of utilised reservoir volume.

Like our theoretical calculation, though, these results should be understood in the broader context of reservoir-scale fluid-rock interaction. In the stirred experimental system the entire, relatively reactive (since freshly ground) pyrite surface area is available to the reacting fluid

and it is, initially, at far from equilibrium conditions. In an actual reservoir, as opposed to our theoretical one, surface availability will depend on pore networks (i.e. the volumes where fluid actually contacts mineral surfaces) and will represent only some fraction of the total mass of pyrite in a given reservoir volume. Where pyrite surfaces are available these will generally have undergone previous fluid-rock interactions and may be less reactive. The system itself, even after introduction of hydrogen, will tend to be closer to equilibrium than the experimental systems presented here and hence overall reactivity will be lower (this is demonstrated in the stirred experiments, where reaction rates tend to fall over the course of the experiment). While the values for hydrogen loss and H_2S production presented here serve as a useful indicator the question of overall reactivity and impact should be addressed through extrapolation of results such as these to more realistic systems, i.e. through modelled or experimental systems containing realistic chemistries and pore-networks.

Due to the reactivity of both hydrogen and pyrite, under certain conditions, the experimental work here was challenging in various ways and has provided us the opportunity to refine and improve experimental and safety systems and procedures along the way. The results from the static experiments in particular highlight the reactivity of pyrite under even slightly oxygenating conditions, which may overprint more subtle changes caused by later reducing conditions. A primary focus in any similar work going forward will therefore be tighter controls on the removal of free oxygen from such systems, along with analytical checks of primary redox-related species and ORP, in order to better characterize and control the redox environment in these systems. Similarly, the results from the reservoir rock-pyrite experiments in particular highlight the far from equilibrium nature of these experiments, which tends to be the primary driver behind reaction, rather than the presence of hydrogen itself. Again, this could mask more subtle changes induced by hydrogen or changes in the redox environment and further experiments utilizing reservoir material could improve the resolution of results by working with equilibrated, or partially equilibrated, rather than far from equilibrium, brines. Finally, it was found that, while each set of experiments focused on analysis complimentary to the types of experiments carried out, full interpretation of the results was hampered where, for example, only characterization of the fluids, as opposed to the solids or gases, was carried out. It is recommended, therefore, that should further, more specific experimental work (geared towards calculation of rate constants, etc., for example) be carried out that all three system components be sampled and characterised as far as possible. While this may necessarily reduce the broad sweep of an experimental program due to time considerations (here, for example, we have focused on covering a wide range of temperatures and solid types which would not have been possible if fuller analysis were undertaken), it would provide benefit in terms of a more detailed interpretation of the results.

In conclusion, the results presented here provide evidence that:

- Reduction of primary pyrite, formation of secondary pyrrhotite and subsequent generation of H_2S can be extensive for pyrite-brine-hydrogen systems at temperatures at or above 120°C.
- Reduction of pyrite is also likely to occur in these systems at a temperature of 80°C, but at a much reduced rate.

These results have implications around H_2S souring of hydrogen streams and corrosion of infrastructure at the field scale and our primary recommendations on this basis are:

- Further experimental and modelling work to better constrain reaction rates and understand their impact at the field-scale.
- Further experimental work to identify if and to what extent these reactions are occurring at lower temperatures (60–100°C).

5 References

Ahn, A. C., A. Hidalgo-Ulloa, Y. Pererva, B. Lomans, and D. Z. }. Sousa. 2022. “Review of the Window of Viability of the Different Microbial Metabolisms Relevant for Subsurface H2 Storage Application.” H2020 HyUSPRe project .

Bateman, Keith, Christopher Rochelle, Alicja Lacinska, and Doris Wagner. 2011. “CO2-Porewater-Rock Reactions - Large-Scale Column Experiment (Big Rig II).” *Energy Procedia* 4: 4937–44.

Belzile, Nelson, Yu-Wei Chen, Mei-Fang Cai, and Yuerong Li. 2004. “A Review on Pyrrhotite Oxidation.” *Journal of Geochemical Exploration* 84 (2): 65–76.

Bourgeois, J. P., N. Aupaix, R. Bloise, and J. L. Millet. 1979. “Proposition d’explication de la formation d’hydrogène sulfuré dans les stockages souterrains de gaz naturel par réduction des sulfures minéraux de la roche magasin.” *Revue de l’Institut francais du Petrole* 34 (3): 371–86.

Carden, P., and L. Paterson. 1979. “Physical, Chemical and Energy Aspects of Underground Hydrogen Storage.” *International Journal of Hydrogen Energy* 4 (6): 559–69.

Cavanagh, A. J., S. H. Yousefi, Wilkinson, and R. M. M & Groenenberg. 2023. “Classifying Hydrogen Storage Potential in Porous Reservoirs as an Aid to Site Selection.” H2020 HyUSPRE Project.

Czernichowski-Lauriol, Isabelle, Chris Rochelle, Irina Gaus, Mohamed Azaroual, Jonathan Pearce, and Pierre Durst. 2006. “Geochemical Interactions between CO2, Pore-Waters and Reservoir Rocks : Lessons Learned from Laboratory Experiments, Field Studies and Computer Simulations.” In *Advances in the Geological Storage of Carbon Dioxide*, edited by S. ;. Altunina Lombardi L.K.; Beaubien S.E. (Eds.).

Foh, Stephen, M. Novil, E. Rockar, and P. Randolph. 1979. “Underground Hydrogen Storage Final Report.” *Inst. Gas Tech. , DOE, Brookhaven Natl Lab, Upton, NY (Dec. 1979)*.

Hassannayebi, Neda, Siroos Azizmohammadi, Marco De Lucia, and Holger Ott. 2019. “Underground Hydrogen Storage: Application of Geochemical Modelling in a Case Study in the Molasse Basin, Upper Austria.” *Environmental Earth Sciences* 78 (5). https://doi.org/10.1007/s12665-019-8184-5.

Reitenbach, Viktor, Leonhard Ganzer, Daniel Albrecht, and Birger Hagemann. 2015. “Influence of Added Hydrogen on Underground Gas Storage: A Review of Key Issues.” *Environmental Earth Sciences* 73 (11): 6927–37.

Thorpe, Arthur N., Frank E. Senftle, Corrinne Alexander, Frank T. Dulong, Robert B. LaCount, and S. Friedman. 1987. “Oxidation of Pyrite in an Anoxic Atmosphere.” *Fuel* 66 (2): 147–53.

Truche, Laurent, Gilles Berger, Christine Destrigneville, Damien Guillaume, and Eric Giffaut. 2010. “Kinetics of Pyrite to Pyrrhotite Reduction by Hydrogen in Calcite Buffered Solutions between 90 and 180°C: Implications for Nuclear Waste Disposal.” *Geochimica et Cosmochimica Acta* 74 (10): 2894–2914.

Truche, Laurent, Gilles Berger, Christine Destrigneville, Alain Pages, Damien Guillaume, Eric Giffaut, and Emmanuel Jacquot. 2009. “Experimental Reduction of Aqueous Sulphate by Hydrogen under Hydrothermal Conditions: Implication for the Nuclear Waste Storage.” *Geochimica et Cosmochimica Acta* 73 (16): 4824–35.

Truche, Laurent, Marie Camille Jodin-Caumon, Catherine Lerouge, Gilles Berger, Régine Mosser-Ruck, Eric Giffaut, and Nicolas Michau. 2013. “Sulphide Mineral Reactions in Clay-Rich Rock Induced by High Hydrogen Pressure. Application to Disturbed or Natural Settings up to 250°C and 30bar.” *Chemical Geology* 351 (August): 217–28.

6 Supporting Information

Full analytical results for the static batch experiments are presented below, each separate table representing an individual ICP-OES run.

	Run			1081		1088	
	Solid			AGH0020		AGH0020	
	Sample type			Pyrite		Pyrite	
	Run time (days)			14		14	
	Run temp. (℃)			80		80	
	Run Pressure (bar)			206		206	
	Gas			H2		N2	
	End pH			3.924		3.723	
	End conductivity (us/cm)			NM		NM	
molar mass	Element	LOD					
		ppm	mol/l	ppm	mol/l	ppm	mol/l
107.87	Ag	*0.00053*	*4.94E-09*	*BD*	*BD*	*BD*	*BD*
26.98	Al	*0.00377*	*1.40E-07*	*0.039*	*1.43E-06*	*10.897*	*4.04E-04*
10.81	B	*0.00085*	*7.84E-08*	*0.057*	*5.31E-06*	*0.066*	*6.09E-06*
137.33	Ba	*0.00007*	*5.18E-10*	*0.304*	*2.21E-06*	*0.267*	*1.95E-06*
40.08	Ca	*0.00081*	*2.02E-08*	*89.876*	*2.24E-03*	*74.525*	*1.86E-03*
112.41	Cd	*0.00032*	*2.83E-09*	*0.014*	*1.23E-07*	*0.024*	*2.16E-07*
140.12	Ce	*0.00113*	*8.08E-09*	*BD*	*BD*	*BD*	*BD*
58.93	Co	*0.00280*	*4.75E-08*	*0.004*	*5.99E-08*	*0.045*	*7.64E-07*
52.00	Cr	*0.00078*	*1.49E-08*	*0.007*	*1.26E-07*	*0.187*	*3.60E-06*
63.55	Cu	*0.01090*	*1.72E-07*	*BD*	*BD*	*BD*	*BD*
55.85	Fe	*0.00051*	*9.20E-09*	*0.011*	*1.92E-07*	*211.896*	*3.79E-03*
69.72	Ga	*NA*	*NA*	*NA*	*NA*	*NA*	*NA*
200.59	Hg	*0.03803*	*1.90E-07*	*BD*	*BD*	*BD*	*BD*
39.10	K	*0.00226*	*5.77E-08*	*23.571*	*6.03E-04*	*23.943*	*6.12E-04*
24.31	Mg	*0.00561*	*2.31E-07*	*0.256*	*1.05E-05*	*4.867*	*2.00E-04*
54.94	Mn	*0.00008*	*1.48E-09*	*BD*	*BD*	*1.172*	*2.13E-05*
22.99	Na	*0.10890*	*4.74E-06*	*13009.636*	*5.66E-01*	*13147.848*	*5.72E-01*
58.69	Ni	*0.00171*	*2.92E-08*	*BD*	*BD*	*0.563*	*9.59E-06*
30.97	P	*0.01006*	*3.25E-07*	*0.452*	*1.46E-05*	*0.196*	*6.33E-06*
207.20	Pb	*0.00520*	*2.51E-08*	*0.153*	*7.39E-07*	*0.086*	*4.16E-07*
32.07	S	*0.02607*	*8.13E-07*	*26.048*	*8.12E-04*	*187.546*	*5.85E-03*
28.09	Si	*0.00492*	*1.75E-07*	*79.711*	*2.84E-03*	*38.506*	*1.37E-03*
87.62	Sr	*0.00002*	*1.84E-10*	*0.205*	*2.34E-06*	*0.361*	*4.12E-06*
47.87	Ti	*0.00004*	*8.72E-10*	*BD*	*BD*	*0.009*	*1.91E-07*
65.38	Zn	*0.00028*	*4.29E-09*	*0.038*	*5.77E-07*	*0.557*	*8.51E-06*
91.22	Zr	*0.00012*	*1.30E-09*	*0.001*	*7.23E-09*	*0.004*	*4.92E-08*

Run		1102		1107		1111		1112		1117		1115		1109		1119		1120	
Solid		AGH0020		AGH0020		AGH0007+AGH0020		AGH0007+AGH0020		AGH0007		AGH0020		AGH0007		AGH0007+AGH0020		AGH0007+AGH0020	
Sample type		Pyrite		Pyrite		R1 + 10% Pyrite		R1 + 20% Pyrite		R1		Pyrite		R1		R1 + 10% Pyrite		R1 + 20% Pyrite	
Run time (days)		14		14		14		14		14		14		14		14		14	
Run temp. (℃)		80		80		80		80		80		80		80		80		80	
Run Pressure (bar)		124		124		124		124		124		124		124		124		124	
Gas		H2		H2		H2		H2		N2		N2		H2		N2		N2	
End pH		5.55		5.157		9.526		9.537		9.409		4.898		9.149		9.377		9.389	
End conductivity (us/cm)		NM		NM		NM		NM		NM		NM		NM		NM		NM	
Element	LoD																		
	ppm	mol/l	ppm	mol/l	ppm	mol/l	ppm	mol/l	ppm	mol/l	ppm	mol/l	ppm	mol/l	ppm	mol/l	ppm	mol/l	ppm	mol/l
Ag	*0.00015*	*1.41E-09*	*BD*	*BD*	*BD*	*BD*	*0.001*	*5.33E-09*	*BD*	*BD*	*0.001*	*7.64E-09*	*0.000*	*2.69E-09*	*0.001*	*4.96E-09*	*0.000*	*4.13E-09*	*BD*	*BD*
Al	*0.77484*	*2.87E-05*	*BD*	*BD*	*BD*	*BD*	*BD*	*BD*	*BD*	*BD*	*BD*	*BD*	*BD*	*BD*	*BD*	*BD*	*BD*	*BD*	*BD*	*BD*
B	*0.00184*	*1.70E-07*	*0.064*	*5.93E-06*	*0.045*	*4.20E-06*	*0.385*	*3.56E-05*	*0.491*	*4.55E-05*	*0.376*	*3.48E-05*	*0.075*	*6.97E-06*	*0.573*	*5.30E-05*	*0.412*	*3.81E-05*	*0.336*	*3.11E-05*
Ba	*0.00014*	*1.00E-09*	*0.073*	*5.32E-07*	*0.048*	*3.49E-07*	*1.574*	*1.15E-05*	*1.981*	*1.44E-05*	*1.527*	*1.11E-05*	*0.067*	*4.89E-07*	*2.239*	*1.63E-05*	*1.607*	*1.17E-05*	*1.439*	*1.05E-05*
Ca	*0.04289*	*1.07E-06*	*17.238*	*4.30E-04*	*12.228*	*3.05E-04*	*100.860*	*2.52E-03*	*141.086*	*3.52E-03*	*92.379*	*2.30E-03*	*15.886*	*3.96E-04*	*154.914*	*3.87E-03*	*111.744*	*2.79E-03*	*105.885*	*2.64E-03*
Cd	*0.00215*	*1.91E-08*	*0.004*	*3.69E-08*	*BD*	*BD*	*BD*	*BD*	*BD*	*BD*	*BD*	*BD*	*0.005*	*4.72E-08*	*BD*	*BD*	*BD*	*BD*	*BD*	*BD*
Ce	*0.00208*	*1.48E-08*	*BD*	*BD*	*BD*	*BD*	*BD*	*BD*	*BD*	*BD*	*BD*	*BD*	*0.019*	*1.37E-07*	*BD*	*BD*	*BD*	*BD*	*BD*	*BD*
Co	*0.00265*	*4.49E-08*	*0.003*	*5.30E-08*	*BD*	*BD*	*BD*	*BD*	*BD*	*BD*	*BD*	*BD*	*0.004*	*6.04E-08*	*BD*	*BD*	*BD*	*BD*	*BD*	*BD*
Cr	*0.00130*	*2.51E-08*	*BD*	*BD*	*BD*	*BD*	*BD*	*BD*	*BD*	*BD*	*BD*	*BD*	*BD*	*BD*	*BD*	*BD*	*BD*	*BD*	*BD*	*BD*
Cu	*0.00132*	*2.07E-08*	*BD*	*BD*	*BD*	*BD*	*BD*	*BD*	*BD*	*BD*	*0.014*	*2.22E-07*	*BD*	*BD*	*BD*	*BD*	*0.009*	*1.35E-07*	*0.005*	*8.59E-08*
Fe	*0.04291*	*7.68E-07*	*86.967*	*1.56E-03*	*62.772*	*1.12E-03*	*BD*	*BD*	*BD*	*BD*	*BD*	*BD*	*103.100*	*1.85E-03*	*BD*	*BD*	*BD*	*BD*	*BD*	*BD*
Ga	*0.00139*	*1.99E-08*	*0.007*	*1.07E-07*	*0.006*	*7.99E-08*	*0.011*	*1.51E-07*	*0.011*	*1.55E-07*	*0.002*	*2.40E-08*	*0.009*	*1.25E-07*	*0.009*	*1.29E-07*	*0.005*	*7.06E-08*	*0.009*	*1.31E-07*
Hg	*0.00444*	*2.22E-08*	*BD*	*BD*	*BD*	*BD*	*0.011*	*5.68E-08*	*0.013*	*6.37E-08*	*BD*	*BD*	*BD*	*BD*	*0.007*	*3.64E-08*	*0.007*	*3.73E-08*	*BD*	*BD*
K	*0.01658*	*4.24E-07*	*18.541*	*4.74E-04*	*12.021*	*3.07E-04*	*341.306*	*8.73E-03*	*416.353*	*1.06E-02*	*355.517*	*9.09E-03*	*16.279*	*4.16E-04*	*469.138*	*1.20E-02*	*390.465*	*9.99E-03*	*325.507*	*8.33E-03*
Mg	*0.02943*	*1.21E-06*	*0.810*	*3.33E-05*	*0.581*	*2.39E-05*	*BD*	*BD*	*BD*	*BD*	*BD*	*BD*	*0.760*	*3.13E-05*	*4.459*	*1.83E-04*	*BD*	*BD*	*BD*	*BD*
Mn	*0.00058*	*1.05E-08*	*1.003*	*1.83E-05*	*0.700*	*1.27E-05*	*BD*	*BD*	*BD*	*BD*	*BD*	*BD*	*0.874*	*1.59E-05*	*BD*	*BD*	*BD*	*BD*	*BD*	*BD*
Na	*0.83841*	*3.65E-05*	*16249.063*	*7.07E-01*	*11693.460*	*5.09E-01*	*11966.575*	*5.21E-01*	*15621.861*	*6.80E-01*	*11310.561*	*4.92E-01*	*14232.281*	*6.19E-01*	*15580.264*	*6.78E-01*	*13284.125*	*5.78E-01*	*11825.276*	*5.14E-01*
Ni	*0.00185*	*3.15E-08*	*BD*	*BD*	*BD*	*BD*	*BD*	*BD*	*BD*	*BD*	*BD*	*BD*	*BD*	*BD*	*BD*	*BD*	*BD*	*BD*	*BD*	*BD*
P	*0.00368*	*1.19E-07*	*0.028*	*8.92E-07*	*0.010*	*3.12E-07*	*0.012*	*3.84E-07*	*0.006*	*1.83E-07*	*BD*	*BD*	*0.009*	*3.06E-07*	*0.015*	*4.88E-07*	*0.011*	*3.41E-07*	*0.010*	*3.10E-07*
Pb	*0.00558*	*2.69E-08*	*BD*	*BD*	*BD*	*BD*	*BD*	*BD*	*BD*	*BD*	*BD*	*BD*	*BD*	*BD*	*0.013*	*6.04E-08*	*BD*	*BD*	*BD*	*BD*
S	*0.13367*	*4.17E-06*	*102.525*	*3.20E-03*	*71.581*	*2.23E-03*	*120.348*	*3.75E-03*	*196.859*	*6.14E-03*	*48.441*	*1.51E-03*	*130.138*	*4.06E-03*	*615.844*	*1.92E-02*	*76.523*	*2.39E-03*	*71.603*	*2.23E-03*
Si	*0.01887*	*6.72E-07*	*8.487*	*3.02E-04*	*5.395*	*1.92E-04*	*123.989*	*4.41E-03*	*169.879*	*6.05E-03*	*113.069*	*4.03E-03*	*7.540*	*2.68E-04*	*115.918*	*4.13E-03*	*134.693*	*4.80E-03*	*114.689*	*4.08E-03*
Sr	*0.00194*	*2.21E-08*	*0.208*	*2.37E-06*	*0.166*	*1.89E-06*	*1.237*	*1.41E-05*	*1.522*	*1.74E-05*	*1.231*	*1.41E-05*	*0.188*	*2.15E-06*	*1.869*	*2.13E-05*	*1.394*	*1.59E-05*	*1.548*	*1.77E-05*
Ti	*0.00355*	*7.41E-08*	*BD*	*BD*	*BD*	*BD*	*BD*	*BD*	*BD*	*BD*	*BD*	*BD*	*BD*	*BD*	*BD*	*BD*	*BD*	*BD*	*BD*	*BD*
Zn	*0.00054*	*8.21E-09*	*0.014*	*2.14E-07*	*0.005*	*7.94E-08*	*BD*	*BD*	*0.001*	*2.07E-08*	*0.003*	*4.80E-08*	*0.523*	*8.01E-06*	*0.004*	*6.75E-08*	*0.002*	*2.97E-08*	*0.002*	*3.64E-08*
Zr	*0.00044*	*4.88E-09*	*0.001*	*1.54E-08*	*0.001*	*7.96E-09*	*BD*	*BD*	*BD*	*BD*	*BD*	*BD*	*0.002*	*2.50E-08*	*BD*	*BD*	*BD*	*BD*	*BD*	*BD*

Run		1134		1136		1140		1142		1144		1146		1151		1148		1149	
Solid		AGH0020		AGH0020		AGH0020+AGH0023		AGH0020+AGH0023		AGH0020+AGH0023		AGH0020		AGH0020+AGH0023		AGH0020+AGH0023		AGH0020	
Sample type		Pyrite		Pyrite		Pyrite + 50% Calcite		Pyrite + 50% Calcite		Pyrite + 50% Calcite		Pyrite		Pyrite 99% + 1% Calcite		Pyrite 99% + 1% Calcite		Pyrite	
Run time (days)		14		14		14		14		14		14		14		14		14	
Run temp. (℃)		120		120		120		120		120		120		120		120		120	
Run Pressure (bar)		103		103		103		103		Vapour pressure		103		103		103		103	
Gas		H2		N2		H2		N2				H2		N2		H2		N2	
End pH		3.651		2.068		7.307		7.436		7.095		2.192		1.462		2.225		2.002	
End conductivity (us/cm)		58609		65210.5		61288.3		61565.2		60170.3		64811		71135.2		64092.2		6480.6	
Element	*LoD*																		
	ppm	mol/l	ppm	mol/l	ppm	mol/l	ppm	mol/l	ppm	mol/l	ppm	mol/l	ppm	mol/l	ppm	mol/l	ppm	mol/l	ppm	mol/l
Ag	*0.00002*	*2.20E-10*	*0.000*	*3.29E-09*	*0.000*	*1.79E-09*	*0.001*	*5.28E-09*	*0.001*	*9.87E-09*	*0.000*	*3.40E-09*	*0.000*	*2.06E-09*	*0.001*	*9.61E-09*	*0.001*	*9.82E-09*	*BD*	*BD*
Al	*0.00413*	*1.53E-07*	*0.203*	*7.52E-06*	*2.303*	*8.53E-05*	*BD*	*BD*	*BD*	*BD*	*BD*	*BD*	*0.541*	*2.00E-05*	*14.637*	*5.42E-04*	*2.270*	*8.41E-05*	*3.390*	*1.26E-04*
B	*0.00373*	*3.45E-07*	*0.251*	*2.32E-05*	*0.315*	*2.91E-05*	*0.042*	*3.93E-06*	*0.038*	*3.47E-06*	*0.057*	*5.26E-06*	*0.724*	*6.70E-05*	*1.113*	*1.03E-04*	*1.443*	*1.33E-04*	*0.782*	*7.23E-05*
Ba	*0.00010*	*7.55E-10*	*0.059*	*4.28E-07*	*0.004*	*2.61E-08*	*0.060*	*4.39E-07*	*0.047*	*3.41E-07*	*0.099*	*7.24E-07*	*0.012*	*9.09E-08*	*0.103*	*7.51E-07*	*0.005*	*3.46E-08*	*0.005*	*3.68E-08*
Ca	*0.00097*	*2.41E-08*	*14.757*	*3.68E-04*	*17.604*	*4.39E-04*	*444.680*	*1.11E-02*	*433.726*	*1.08E-02*	*436.427*	*1.09E-02*	*19.637*	*4.90E-04*	*177.756*	*4.44E-03*	*170.565*	*4.26E-03*	*13.636*	*3.40E-04*
Cd	*0.00039*	*3.49E-09*	*0.036*	*3.25E-07*	*0.042*	*3.70E-07*	*BD*	*BD*	*0.001*	*6.87E-09*	*BD*	*BD*	*0.108*	*9.61E-07*	*0.205*	*1.83E-06*	*0.274*	*2.44E-06*	*0.102*	*9.04E-07*
Ce	*0.00199*	*1.42E-08*	*BD*	*BD*	*0.021*	*1.48E-07*	*BD*	*BD*	*BD*	*BD*	*BD*	*BD*	*0.008*	*5.58E-08*	*0.006*	*4.19E-08*	*0.004*	*2.59E-08*	*0.033*	*2.32E-07*
Co	*0.00064*	*1.08E-08*	*0.001*	*1.47E-08*	*0.006*	*9.65E-08*	*0.002*	*2.61E-08*	*0.003*	*4.62E-08*	*0.002*	*4.15E-08*	*0.009*	*1.46E-07*	*0.004*	*7.60E-08*	*0.001*	*1.17E-08*	*0.015*	*2.49E-07*
Cr	*0.00114*	*2.19E-08*	*BD*	*BD*	*BD*	*BD*	*BD*	*BD*	*BD*	*BD*	*BD*	*BD*	*0.004*	*6.76E-08*	*0.018*	*3.53E-07*	*0.005*	*9.43E-08*	*0.008*	*1.61E-07*
Cu	*0.00041*	*6.46E-09*	*BD*	*BD*	*BD*	*BD*	*BD*	*BD*	*BD*	*BD*	*BD*	*BD*	*BD*	*BD*	*BD*	*BD*	*BD*	*BD*	*BD*	*BD*
Fe	*0.00054*	*9.65E-09*	*404.442*	*7.24E-03*	*441.368*	*7.90E-03*	*0.216*	*3.87E-06*	*0.158*	*2.83E-06*	*0.173*	*3.10E-06*	*730.164*	*1.31E-02*	*834.515*	*1.49E-02*	*859.932*	*1.54E-02*	*713.392*	*1.28E-02*
Ga	*NA*	*NA*	*NA*	*NA*	*NA*	*NA*	*NA*	*NA*	*NA*	*NA*	*NA*	*NA*	*NA*	*NA*	*NA*	*NA*	*NA*	*NA*	*NA*	*NA*
Hg	*0.00142*	*7.07E-09*	*BD*	*BD*	*BD*	*BD*	*BD*	*BD*	*BD*	*BD*	*BD*	*BD*	*0.006*	*3.08E-08*	*BD*	*BD*	*0.007*	*3.56E-08*	*0.006*	*3.12E-08*
K	*0.00006*	*1.42E-09*	*12.997*	*3.32E-04*	*18.739*	*4.79E-04*	*18.879*	*4.83E-04*	*17.233*	*4.41E-04*	*19.932*	*5.10E-04*	*34.628*	*8.86E-04*	*22.050*	*5.64E-04*	*16.166*	*4.13E-04*	*37.484*	*9.59E-04*
Mg	*0.00138*	*5.66E-08*	*1.713*	*7.05E-05*	*2.954*	*1.22E-04*	*9.650*	*3.97E-04*	*7.482*	*3.08E-04*	*8.162*	*3.36E-04*	*6.308*	*2.60E-04*	*6.749*	*2.78E-04*	*7.603*	*3.13E-04*	*6.810*	*2.80E-04*
Mn	*0.00008*	*1.52E-09*	*0.424*	*7.71E-06*	*0.516*	*9.40E-06*	*0.032*	*5.81E-07*	*0.027*	*4.96E-07*	*0.037*	*6.66E-07*	*0.323*	*5.88E-06*	*1.087*	*1.98E-05*	*1.158*	*2.11E-05*	*0.268*	*4.88E-06*
Na	*0.10887*	*4.74E-06*	*8827.479*	*3.84E-01*	*9467.394*	*4.12E-01*	*9298.625*	*4.04E-01*	*9033.709*	*3.93E-01*	*9591.882*	*4.17E-01*	*8735.849*	*3.80E-01*	*8418.257*	*3.66E-01*	*8680.104*	*3.78E-01*	*9134.928*	*3.97E-01*
Ni	*0.00202*	*3.44E-08*	*BD*	*BD*	*BD*	*BD*	*0.003*	*4.53E-08*	*0.005*	*8.16E-08*	*BD*	*BD*	*0.003*	*4.48E-08*	*BD*	*BD*	*BD*	*BD*	*0.005*	*9.23E-08*
P	*0.00373*	*1.21E-07*	*0.050*	*1.61E-06*	*0.084*	*2.72E-06*	*0.029*	*9.47E-07*	*0.036*	*1.15E-06*	*0.028*	*8.95E-07*	*0.059*	*1.89E-06*	*0.204*	*6.59E-06*	*0.106*	*3.42E-06*	*0.075*	*2.42E-06*
Pb	*0.00108*	*5.19E-09*	*BD*	*BD*	*BD*	*BD*	*BD*	*BD*	*BD*	*BD*	*0.005*	*2.42E-08*	*BD*	*BD*	*0.032*	*1.52E-07*	*0.020*	*9.88E-08*	*BD*	*BD*
S	*0.02922*	*9.11E-07*	*609.712*	*1.90E-02*	*774.793*	*2.42E-02*	*722.525*	*2.25E-02*	*707.283*	*2.21E-02*	*735.523*	*2.29E-02*	*1747.960*	*5.45E-02*	*4338.039*	*1.35E-01*	*4542.189*	*1.42E-01*	*1863.316*	*5.81E-02*
Si	*0.00935*	*3.33E-07*	*117.283*	*4.18E-03*	*124.185*	*4.42E-03*	*129.781*	*4.62E-03*	*119.147*	*4.24E-03*	*126.981*	*4.52E-03*	*183.185*	*6.52E-03*	*68.462*	*2.44E-03*	*44.206*	*1.57E-03*	*186.223*	*6.63E-03*
Sr	*0.00055*	*6.29E-09*	*0.125*	*1.43E-06*	*0.068*	*7.75E-07*	*1.637*	*1.87E-05*	*1.406*	*1.60E-05*	*1.446*	*1.65E-05*	*0.046*	*5.22E-07*	*0.422*	*4.81E-06*	*0.252*	*2.88E-06*	*0.036*	*4.14E-07*
Ti	*0.00007*	*1.47E-09*	*0.000*	*1.95E-09*	*0.003*	*5.55E-08*	*BD*	*BD*	*BD*	*BD*	*BD*	*BD*	*0.001*	*1.54E-08*	*0.069*	*1.44E-06*	*0.001*	*2.25E-08*	*0.003*	*6.60E-08*
Zn	*0.00021*	*3.19E-09*	*0.048*	*7.39E-07*	*0.380*	*5.82E-06*	*0.006*	*8.87E-08*	*0.004*	*6.87E-08*	*0.004*	*6.67E-08*	*0.196*	*3.00E-06*	*0.518*	*7.92E-06*	*0.358*	*5.47E-06*	*0.311*	*4.75E-06*
Zr	*0.00014*	*1.53E-09*	*0.005*	*5.51E-08*	*0.006*	*6.18E-08*	*0.004*	*4.59E-08*	*0.002*	*2.70E-08*	*0.004*	*3.93E-08*	*0.012*	*1.36E-07*	*0.024*	*2.58E-07*	*0.029*	*3.22E-07*	*0.014*	*1.50E-07*